https://doi.org/10.1093/plcell/koad053 THE PLANT CELL 2023: 1–29

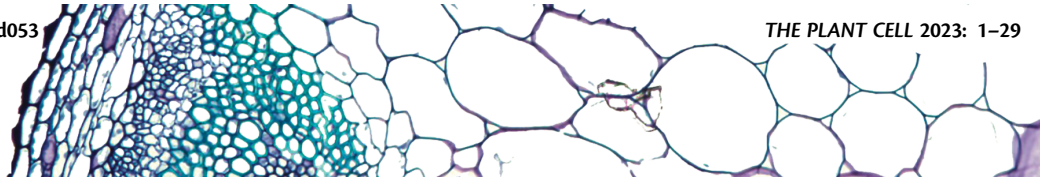

Research Article

Loss of OPT3 function decreases phloem copper levels and impairs crosstalk between copper and iron homeostasis and shoot-to-root signaling in *Arabidopsis thaliana*

Ju-Chen Chia [1], Jiapei Yan [1], Maryam Rahmati Ishka [1,5], Marta Marie Faulkner [1], Eli Simons [1], Rong Huang [3], Louisa Smieska [3], Arthur Woll [3], Ryan Tappero [4], Andrew Kiss [4], Chen Jiao [5], Zhangjun Fei [5,6], Leon V. Kochian [6,†], Elsbeth Walker [7], Miguel Piñeros [2,5,6] and Olena K. Vatamaniuk [1,2,*]

1 Soil and Crop Sciences Section, School of Integrative Plant Science, Cornell University, Ithaca, NY 14853, USA
2 Plant Biology Section, School of Integrative Plant Science, Cornell University, Ithaca, NY 14853, USA
3 Cornell High Energy Synchrotron Source (CHESS), Cornell University, Ithaca, NY 14853, USA
4 National Light Source II, Brookhaven National Laboratory, Upton, NY 11973, USA
5 Boyce Thompson Institute for Plant Research, Ithaca, NY 14853, USA
6 Robert W. Holley Center for Agriculture and Health, USDA-ARS, NY 14853, USA
7 Department of Biology, University of Massachusetts, MA 01003, USA

*Author for correspondence: E-mail: okv2@cornell.edu (O.K.V.)
†Present address: Global Institute for Food Security, University of Saskatchewan, Saskatoon, Canada.
The author responsible for the distribution of material integral to the findings presented in this article in accordance with the policy described in the Instructions for Authors (https://academic.oup.com/plcell/) is Olena Vatamaniuk (okv2@cornell.edu)

Abstract

Copper (Cu) and iron (Fe) are essential micronutrients that are toxic when accumulating in excess in cells. Thus, their uptake by roots is tightly regulated. While plants sense and respond to local Cu availability, the systemic regulation of Cu uptake has not been documented in contrast to local and systemic control of Fe uptake. Fe abundance in the phloem has been suggested to act systemically, regulating the expression of Fe uptake genes in roots. Consistently, shoot-to-root Fe signaling is disrupted in *Arabidopsis thaliana* mutants lacking the phloem companion cell-localized Fe transporter, OLIGOPEPTIDE TRANSPORTER 3 (AtOPT3). We report that AtOPT3 also transports Cu in heterologous systems and contributes to its delivery from sources to sinks in planta. The *opt3* mutant contained less Cu in the phloem, was sensitive to Cu deficiency and mounted a transcriptional Cu deficiency response in roots and young leaves. Feeding the *opt3* mutant and Cu- or Fe-deficient wild-type seedlings with Cu or Fe via the phloem in leaves downregulated the expression of both Cu- and Fe-deficiency marker genes in roots. These data suggest the existence of shoot-to-root Cu signaling, highlight the complexity of Cu/Fe interactions, and the role of AtOPT3 in fine-tuning root transcriptional responses to the plant Cu and Fe needs.

Introduction

Iron (Fe) and copper (Cu) are essential elements that are required in trace amounts to complete the life cycle of all organisms, including plants and humans. However, these elements are toxic to cells if they accumulate in their free ionic forms (Broadley et al. 2012; Ravet and Pilon 2013). The essential yet toxic nature of Fe and Cu is attributed to the ease with which they accept and donate electrons

Received July 21, 2022. Accepted February 17, 2023. Advance access publication February 23, 2023

(Broadley et al. 2012; Ravet and Pilon 2013). This ability has been capitalized by nature, as Cu- and Fe-containing enzymes are required for vital physiological reactions, including photosynthesis, respiration and scavenging reactive oxygen species (Broadley et al. 2012; Ravet and Pilon 2013). In addition, Cu is required for cell wall lignification and reproduction (Epstein and Bloom 2005; Broadley et al. 2012; Chen et al. 2020; Rahmati Ishka and Vatamaniuk 2020; Sheng et al. 2021; Perez-Anton et al. 2022; Rahmati Ishka et al. 2022; Vatamaniuk 2022). Recent studies implicate Cu in light-dependent seed germination (Jiang et al. 2021), shaping the shoot architecture, transition to flowering, stigmatic papillae development, and senescence (Ishka and Vatamaniuk 2020; Sheng et al. 2021), as recently reviewed in (Rahmati Ishka et al. 2022). Mounting evidence from studies in animal species suggests that in addition to a static function as a cofactor of cellular enzymes, Cu is involved in cell signaling (Turski and Thiele 2009; Turski et al. 2012; Chang 2015; Tsang et al. 2020). In plants, Cu participates in phytohormone signaling and accumulation. Specifically, Cu(I) in the transmembrane sensor domain of the ethylene receptor ETHYLENE RESPONSE 1 (ETR1) is essential for ethylene binding and receptor function in ethylene signaling in Arabidopsis (*Arabidopsis thaliana*) (Rodríguez et al. 1999; Schott-Verdugo et al. 2019). Likewise, the binding of the plant defense hormone salicylic acid to its receptor NONEXPRESSER OF PR GENES 1 (NPR1) occurs via Cu; moreover, Cu deficiency increases the accumulation of jasmonic acid in Arabidopsis leaves (Wu et al. 2012; Yan et al. 2017; Rahmati Ishka et al. 2022). Fe-containing enzymes are also involved in nitrate and sulfate assimilation, chlorophyl biosynthesis, and ethylene and jasmonic acid accumulation (Broadley et al. 2012; Li and Lan 2017; Cui et al. 2018).

Cu and Fe uptake by plant roots and their internal transport and storage are rigorously regulated at transcriptional and posttranscriptional levels in response to their availability in the local environment and the demands of the developing shoot (Burkhead et al. 2009; Ravet and Pilon 2013; Kobayashi 2019; Pottier et al. 2019; Spielmann and Vert 2020). To maintain Cu homeostasis, plants regulate cellular Cu uptake and economize Cu use by prioritizing it during deficiency from non-essential to essential Cu enzymes (Burkhead et al. 2009; Ravet and Pilon 2013; Rahmati Ishka et al. 2022). In Arabidopsis, both mechanisms are controlled by a conserved transcription factor, SPL7 (SQUAMOSA PROMOTER BINDING PROTEIN–LIKE7) (Yamasaki et al. 2009; Bernal et al. 2012). In addition to SPL7, a member of the basic helix-loop-helix (bHLH) family, CITF1 (CU DEFICIENCY-INDUCED TRANSCRIPTION FACTOR 1, also named bHLH160) regulates Cu uptake from roots, delivery to leaves, flowers, and anthers (Yan et al. 2017). CITF1 acts together with SPL7, and both are required for Cu delivery to reproductive organs and fertility (Yan et al. 2017). The SPL7-dependent regulon also includes the *Fe/Cu REDUCTASE OXIDASE* genes *FRO4* and *FRO5*; several Cu transporter genes, including *COPT1*, *COPT2* and, in part, *COPT6*, which encode members of the CTR/COPT/SLC31 (CU TRANSPORTER/CU TRANSPORTER/SOLUTE CARRIER 31) family; *CITF1* and the uncharacterized transcription factor gene *bHLH23* (also named *CITF2*) (Yamasaki et al. 2009; Bernal et al. 2012; Jung et al. 2012; Gayomba et al. 2013; Jain et al. 2014; Araki et al. 2018; Alexander et al. 2019; Schulten et al. 2022). *FRO4/5* and *COPT2* are also downstream targets of CITF1 (Yan et al. 2017). The altered expression of SPL7- and CITF1-regulated genes and the increased expression of *CITF1* constitute a signature of the Cu deficiency response. Recent studies have shown that *SPL7* is expressed mainly in the Arabidopsis vasculature and locally regulates root and shoot responses to Cu deficiency (Araki et al. 2018). The existence of long-distance Cu signaling has not yet been reported.

Regulation of Fe homeostasis in Arabidopsis involves a network of transcription factors from the bHLH family (Jeong et al. 2017; Kim et al. 2019). Specifically, a member of the IVb subgroup of the bHLH family, URI (UPSTREAM REGULATOR OF IRT1, identical to bHLH121), acts upstream as an Fe-dependent switch (Kim et al. 2019; Gao et al. 2020). URI heterodimerizes with a subgroup IVc bHLH member to regulate the expression of the master regulator of Fe homeostasis *FIT* (*FER-LIKE FE DEFICIENCY-INDUCED TRANSCRIPTION FACTOR*, also named *bHLH29*) (Kim et al. 2019; Gao et al. 2020). FIT forms heterodimers with Ib subgroup bHLH transcription factors to regulate the expression of multiple genes in Arabidopsis roots, among which are some components of the Fe uptake system, *IRT1* (*FE-REGULATED TRANSPORTER 1*), *FRO2*, and *AHA2* [*ARABIDOPSIS* H^+*-ATPASE*], reviewed in Jeong et al. (2017) and Schwarz and Bauer (2020)). The upregulated expression of Ib bHLH genes, *FIT*, *AHA2*, *FRO2*, and *IRT1*, and the newly discovered *IMA/FEP* Fe-sensing peptide genes (*FE MAN* [*IMA*]*/FE UPTAKE-INDUCING PEPTIDE* [*FEP*]) is a hallmark of the root Fe deficiency response (Jeong et al. 2017; Grillet et al. 2018; Hirayama et al. 2018; Schwarz and Bauer 2020). These and other Fe-responsive genes are upregulated in response to local and systemic Fe status signals (Gayomba et al. 2015; Jeong et al. 2017; Grillet et al. 2018; Hirayama et al. 2018; Schwarz and Bauer 2020).

Several mutants with disrupted shoot-to-root Fe deficiency signaling have been identified in Arabidopsis and other plant species. All exhibit constitutive activation of Fe-acquisition genes even when grown under Fe-sufficient conditions (Garcia et al. 2013; Kumar et al. 2017) and reviewed in Gayomba et al. (2015). Of these, a member of the OPT (OLIGO PEPTIDE TRANSPORTER) clade of the OPT transporter family, Arabidopsis OPT3, is considered a key player in the systemic signaling of Fe deficiency (Stacey et al. 2002, 2008; Mendoza-Cózatl et al. 2014; Zhai et al. 2014). While the *opt3-1* knockout allele is embryo-lethal, the *opt3-2* and *opt3-3* alleles possess residual levels of *OPT3* expression and overaccumulate Fe in roots and leaves because they cannot appropriately downregulate the expression of *AHA2*, *IRT1*, *FRO2*, or other Fe deficiency-responsive

genes (Stacey et al. 2002, 2008; Mendoza-Cózatl et al. 2014; Zhai et al. 2014). Arabidopsis OPT3 can mediate Fe uptake into *Xenopus laevis* oocytes and budding yeast (*Saccharomyces cerevisiae*), localizes to companion cells of the phloem, mediates Fe loading to the phloem, and facilitates Fe delivery from sources (mature leaves) to sinks (roots and seeds) (Zhai et al. 2014). Based on these findings, OPT3 has been suggested to communicate the Fe sufficiency status to the root by loading Fe into the phloem companion cells in leaves. Consistent with this suggestion, the loss of the Fe transport function in the *opt3-3* mutant and the decreased Fe accumulation in its phloem sap not only led to a lower accumulation of Fe in seeds but also is perceived as the Fe deficiency signal by roots (Zhai et al. 2014). Local sensing of high Fe status in the shoot does not seem to be disrupted in weak *opt3* mutants, as evidenced by the increased expression of genes encoding the Fe-storage proteins FERRITIN 3 (FER3) and FER4 (Khan et al. 2018).

Fe abundance or a lack thereof in plant tissues is tightly linked to the accumulation of other transition metals (Baxter et al. 2008). In this regard, the crosstalk between Fe and Cu is now well documented. The hallmark of this crosstalk is the overaccumulation of Cu under Fe deficiency conditions and the overaccumulation of Fe under Cu deficiency conditions (Bernal et al. 2012; Waters and Armbrust 2013; Kastoori Ramamurthy et al. 2018; Rai et al. 2021; Sheng et al. 2021). FIT and the bHLH Ib group transcription factors (bHLH38, bHLH39, bHLH100, and bHLH101) have also been shown to control the upregulation of Cu uptake genes (*COPT2*, *FRO4*, and *FRO5*) under Fe-deficiency and Cu is required for improving plant growth under Fe-deficiency conditions (Colangelo and Guerinot 2004; Cai et al. 2021). Consistent with the increased Cu uptake, the expression of Cu-deficiency-regulated genes is downregulated under Fe deficiency (Waters et al. 2012, 2014; Yan et al. 2017). Conversely, Fe overaccumulation can also decrease Cu uptake in Arabidopsis and animal systems (Klevay 2001; Waters and Armbrust 2013; Ha et al. 2016). Together, these studies suggest that Cu and Fe homeostasis are interconnected and that deficiency for one of the metals or both can interfere with their local and/or long-distance status signaling.

Here we provide evidence that in addition to Fe, Arabidopsis OPT3 mediates Cu uptake into *Xenopus* oocytes and yeast cells. Loss of OPT3 function in the *opt3-3* mutant results in decreased Cu accumulation in the phloem and diminished Cu recirculation from sources (mature leaves) to sinks (young leaves and the seed coat of developing seeds) compared to the wild-type. In addition, the *opt3-3* mutant experiences Cu deficiency, as evidenced by low Cu accumulation in its roots and young leaves and the increased expression of Cu-deficiency marker genes in these tissues. Importantly, these defects are rescued by Cu application. Furthermore, Cu feeding via the phloem in the shoot rescued the molecular symptoms of Cu deficiency in the root of the wild-type and the *opt3-3* mutant, suggesting the existence of long-distance shoot-to-root Cu signaling. This suggestion is further strengthened by results from reciprocal grafting experiments using wild-type and the *opt3-3* mutant. Interestingly, phloem-feeding with Cu in the shoot also rescued molecular symptoms of Fe deficiency in the root of the *opt3-3* mutant and decreased the transcript abundance of molecular markers of Fe deficiency in the root of wild-type. Likewise, phloem-feeding with Fe in the shoot downregulated the expression of both Fe- and Cu-deficiency marker genes in the root of the *opt3-3* mutant or wild-type. These data assign new transport capabilities to AtOPT3, suggest the existence of shoot-to-root signaling of Cu status, and highlight the complexity of the crosstalk between Cu and Fe in long-distance signaling.

Results

Mineral distribution has changed in the vasculature of the *opt3-3* mutant, and the mutant accumulates less cu in the phloem

Arabidopsis OPT3 localizes to the plasma membrane, associates with the phloem (Fig. 1A and (Mendoza-Cózatl et al. 2014; Zhai et al. 2014)), resides in phloem companion cells (Mustroph et al. 2009), and facilitates Fe accumulation in the phloem, likely via xylem-to-phloem transfer (Zhai et al. 2014). As a result of this function, Fe concentration in the phloem sap is significantly lower, while it is considerably higher in the xylem sap in the *opt3-3* mutant compared to the wild-type (Zhai et al. 2014). Here, we used synchrotron X-ray fluorescence (XRF) microscopy to compare the spatial distribution of Fe and other elements in the vasculature of the *opt3-3* mutant (referred to as *opt3* thereafter) and in the wild-type. We first evaluated mineral distribution in mature leaves, which serve as photosynthetic sources of nutrients for developing leaves at the vegetative stage. Consistent with our previous findings (Zhai et al. 2014), the *opt3* mutant accumulated more Fe throughout the leaf blade compared to the wild-type, with the bulk of Fe located in minor veins (Fig. 1B and Supplemental Fig. S1, A to D). We also found that in addition to Fe, mature leaves of the *opt3* mutant accumulate more Cu (Fig. 1C and Supplemental Fig. S1, A to D), manganese (Mn), and zinc (Zn) (Fig. 1C to E). Mn and Zn were spread throughout the leaf blade of the wild-type, including the vasculature, with the highest accumulation in basal cells of trichomes (Fig. 1, D, E, H, I and K). Cu also accumulated in the vasculature of the *opt3* mutant, and its distribution pattern in minor veins resembled the distribution of Fe (Fig. 1, B, C and K, and Supplemental Fig. S1, A to D).

We then used 2D-XRF in confocal mode (2D-CXRF) with a specialized x-ray collection optic to obtain a micron-scale resolution; this setup enabled comparative analyses of mineral localization in the phloem and the xylem of the *opt3* mutant and the wild-type. For the current study, this technique is preferable to traditional XRF methods (both 2D-XRF and 3D micro-XRF tomography) because it allows quantitative

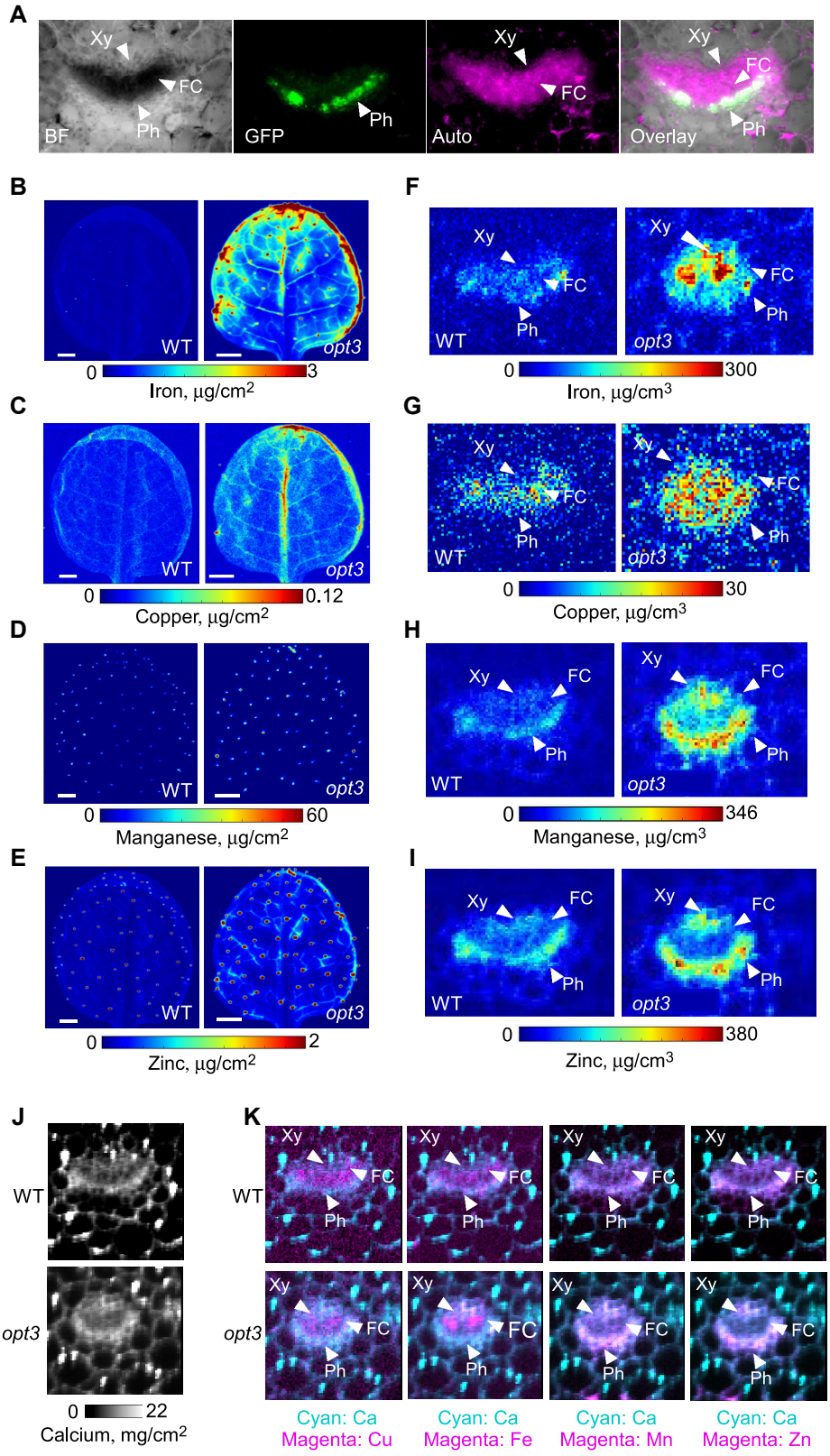

Figure 1. OPT3 mediates Cu loading to the phloem. **A)** Hand-cut cross sections through the petiole of transgenic wild-type plants expressing the *OPT3pro:GFP* construct (Zhai et al. 2014). **B to E)** 2D-XRF maps of the indicated minerals in mature leaves. **F to J)** 2D-CXRF maps of the indicated elements in the vasculature of mature leaf petioles. **K)** Merged images of calcium (Ca) and indicated elements. Ca maps show the overall structures of the vascular tissues of the wild-type (WT) and the *opt3-3* mutant (*opt3*), and that the majority of Cu and Fe in the mutant is associated with the xylem and fascicular cambium (FC). Plants were grown hydroponically with 250 nM $CuSO_4$ for 26 d (in B to E) or 5 wk (in F to I) before tissues were collected. In B to K, scale bars, 1 mm. Xy xylem; FC, fascicular cambium; Ph, phloem. **B to K)** Representative images from three analyzed plants. Results from other independent experiments are shown in Supplemental Fig. S1C to J.

comparisons of metal distributions among different samples without the need to control or limit sample thickness or lateral size (Mantouvalou et al. 2012). Using 2D-CXRF, we determined that the spatial distribution of elements is altered in the *opt3* mutant compared to the wild-type (Fig. 1, F, I and K and Supplemental Fig. S1E to J). We validated this result by comparing the distribution of fluorescence from calcium (Ca, used to visualize cell boundaries, [Fig. 1J and Supplemental Fig. S1I]) overlayed with the fluorescence from Fe or Cu, Zn, or Mn (Fig. 1K). Specifically, while Fe was either evenly distributed between the xylem and the phloem regions or was found more towards the phloem in the wild-type, the bulk of Fe was associated more towards the xylem and fascicular cambium region and to a lesser extent in the phloem region in the *opt3* mutant (Fig. 1, F and K and Supplemental Fig. S1, E and J). The concentration of Mn and Zn was higher in the phloem than the xylem in the wild-type and increased in both the xylem and the phloem of the *opt3* mutant (Fig. 1, H, I and K and Supplemental Fig. S1G, H and J). Cu was mainly located in the fascicular cambium and phloem regions and, to a lesser extent, the xylem in the wild-type (Fig. 1, G and K and Supplemental Fig. S1, F and J). By contrast, the bulk of Cu was associated with the xylem and fascicular cambium and, to a lesser extent, the phloem tissues in the *opt3* mutant (Fig. 1, G and K and Supplemental Fig. S1F and J).

Consistent with 2D-CXRF results, the concentration of Cu in the phloem was significantly lower in the *opt3* mutant compared with the wild-type (Fig. 2A). The decreased accumulation of Cu in the phloem of the *opt3* mutant relative to the wild-type was independently found by the Walker lab (Supplemental Fig. S1K).

Roots, young leaves, and the seed coat of developing seeds of the *opt3* mutant accumulate less Cu

Past studies have shown that mutant alleles of *OPT3* overaccumulate Fe, Mn, and Zn in their roots and leaves (Stacey et al. 2008; Mendoza-Cózatl et al. 2014; Zhai et al. 2014). Since the 2D-CXRF analysis of mineral distribution in the vasculature also pointed to the role of OPT3 in Cu homeostasis, we refined our past study of total internal metal accumulation to include Cu. Consistent with past findings, roots and both mature and young leaves of the *opt3* mutant accumulated significantly more Fe, Mn, and Zn compared to the corresponding organs of the wild-type (Supplemental Fig. S2). By contrast, the concentration of Cu in the roots of the *opt3* mutant was less than 1/3 of the wild-type levels (Fig. 2A). We also found that the Cu concentration was higher in mature leaves (sources) and lower in young leaves (sinks) in the *opt3* mutant compared to the wild-type (Fig. 2A). We obtained similar results using the independent *opt3-2* allele (Supplemental Fig. S3).

We then analyzed the accumulation and distribution of Cu, Fe, Mn, and Zn in other source tissues, such as silique valves and their sinks, developing and mature seeds. Inductively coupled plasma–mass spectrometry (ICP-MS) analysis determined that silique valves of the *opt3* mutant overaccumulate Cu, Fe, Mn, and Zn compared to the wild-type (Fig. 2B). Using 2D-XRF, we found that developing seeds of the mutant accumulate less Cu and Fe (Fig. 2C and Supplemental Fig. S4A) but more Mn and Zn relative to the wild-type (Fig. 2C), suggesting that Cu and Fe delivery from sources to sinks is lower in the mutant. Indeed, the spatial distribution of Cu detectable by 2D-XRF in developing seeds of both wild-type and the *opt3* mutant was distinct from that of Fe. Specifically, Cu was associated primarily with the seed coat of the developing seed, while Fe mainly localized in the embryo vasculature.

We also used high-resolution Synchrotron-based XRF Computed Microtomography (F-CMT) to visualize minerals in mature seeds. Similar to embryos, Cu was associated mainly with the seed coat and was detected throughout the seed and the vasculature (Supplemental Fig. S4B). We observed little to no difference in Cu accumulation in the seed coat of the mature seed of the mutant relative to the wild-type, while the Cu concentration in the vasculature appeared to be lower in the *opt3* mutant than the wild-type (Supplemental Fig. S4B). Total Cu concentrations in mature seeds were similar in both genotypes (Supplemental Fig. S4C). As was shown previously, Fe was associated with vascular parenchyma cells in mature wild-type seeds (Supplemental Fig. S4B and (Kim et al. 2006)). Fe distribution did not change in the mutant, although Fe levels in *opt3* vascular parenchyma cells were significantly lower than in the wild-type. Consistently, total internal Fe concentration was lower in *opt3* mutant seeds compared to the wild-type (Supplemental Fig. S4C). While the distribution of Mn and Zn did not change in the mutant relative to the wild-type, *opt3* mutant seeds accumulated significantly more Zn (Supplemental Fig. S4,B and C). Together, our data suggest that OPT3 contributes to the phloem-based redistribution of Cu from mature leaves to young leaves and from silique valves to developing seeds (most detectible at the seed coat). Therefore, in addition to Fe, AtOPT3 may also transport Cu.

OPT3 mediates Cu uptake in *Xenopus* oocytes and yeast

We assessed the ability of OPT3 to transport Cu in *Xenopus laevis* oocytes, as we previously showed that OPT3 localizes to the plasma membrane and mediates Fe and cadmium (Cd) ions uptake into oocytes (Zhai et al. 2014). We tested Cu^{2+} (provided as $CuSO_4$) and Cu complexed with its biological ligand, nicotianamine (Cu–NA) as potential transport substrates. We observed that OPT3 transports both free Cu^{2+} ions and Cu provided as a Cu–NA complex into oocytes (Fig. 3A). However, *OPT3*-expressing oocytes contained 4.2 times more Cu when it was provided as the free ion than when complexed with NA. This finding suggested that free Cu^{2+} ions are a preferred OPT3 substrate, at least in this

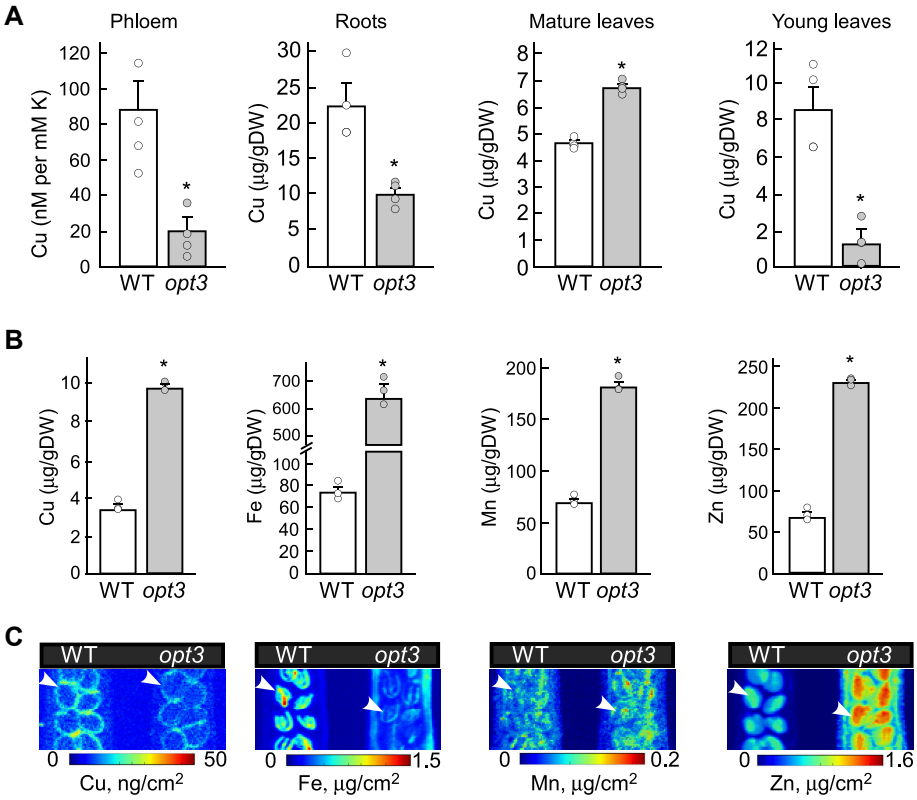

Figure 2. The *opt3-3* mutant accumulates less Cu in the phloem sap, roots, young leaves and the seed coat of developing seeds than wild-type. **A)** Cu concentration in the phloem sap and the indicated plant tissues of the wild-type and the *opt3-3* (*opt3*) mutant. Plants were grown hydroponically under Fe- and Cu-sufficient conditions. Values are means ± SE. Asterisks indicate statistically significant differences from wild-type ($P < 0.05$, Student's *t*-test, $n = 4$ independent phloem sap collections or four independent ICP-MS experiments. In each experiment, tissues were collected from 4 to 5 plants grown in the same container). An independent analysis of Cu concentration in the phloem sap in the *opt3-3* allele and Cu and Other elemental concentrations in tissues of the second allele *opt3-2* are shown in Supplemental Fig. S1E and SS3, respectively. **B)** ICP-MS analysis of mineral accumulation in dry silique valves collected from soil-grown plants. Values are means ± SE. Asterisks indicate statistically significant differences from the wild-type ($P < 0.05$, Student's *t*-test, $n = 3$ independent experiments. In each experiment, tissues from four to five plants grown in the same container were pooled and represented an independent measurement. Data for the wild-type and the *opt3-2* allele are shown in Supplemental Fig. S3. **C)** Representative 2D-SXRF images of siliques from wild-type and *opt3*. Fifteen-mm-long developing siliques were collected from soil-grown plants and subjected to 2D-SXRF analysis. White arrows point to embryos. A representative image from three independent experiments is shown; results from the other two independent experiments are shown in Supplemental Fig. S4A.

heterologous system. Visual examination and membrane potential measurements allowed us to assess the cellular integrity of mock and *OPT3*-expressing oocytes throughout uptake experiments to rule out the possibility that the observed fluxes were the product of membrane leakiness due to cellular Cu toxicity rather than specific OPT3-mediated Cu uptake (Supplemental Fig. S5). Under control conditions, the membrane potential of cells expressing *OPT3* was about 20 mV less negative than that recorded from mock cells, consistent with our earlier reports (Zhai et al. 2014). Exposure to the Cu^{2+}-containing uptake solution for 3 h did not change the appearance or survival rates of mock and *OPT3*-expressing oocytes (Supplemental Fig. S5A). Under these conditions, mock cells experienced only a small gain in membrane potential (from −57 ± 1 mV to −50 ± 1 mV), and a slightly larger change in the same direction recorded for *OPT3*-expressing cells (from −35 ± 4 mV to −21 ± 4 mV). After transferring cells into Cu-free solution, the survival rates of *OPT3*-expressing cells, but not those of mock-treated cells, dramatically decreased over the next 21 h of incubation in Cu-free medium (Supplemental Fig. S5A). The decreased survival rates were associated with the significant increase in the membrane potential in the OPT3-expressing vs. mock-treated cells (Supplemental Fig. S5A). Decreased survival rates and increased membrane potential in the OPT3-expressing oocytes vs. mock-treated cells was observed after long-term (24 h) but not short-term (3 h) incubation with Cu (Supplemental Fig. S5B). We conclude that the drop in the survival rates of *OPT3*-expressing cells resulted from OPT3-mediated Cu accumulation, leading to cellular toxicity, which was manifested by a loss in cellular ability to maintain a resting potential, leading to eventual cell death.

We further validated the ability of OPT3 to transport Cu by functional complementation assays in budding yeast, which does not synthesize NA. We used the Cu-deficient yeast mutant *ctr1Δctr2Δctr3Δ* lacking the high-affinity plasma

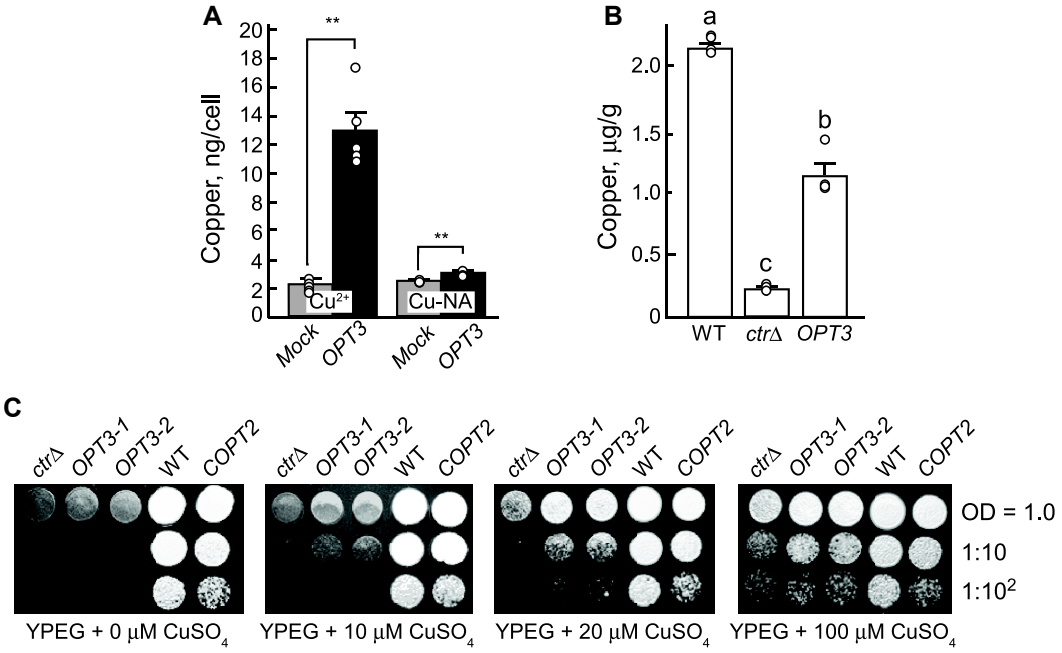

Figure 3. OPT3 transports Cu in *X. laevis* oocytes and *S. cerevisiae*. **A)** Cu uptake into *Xenopus* oocytes injected with either *OPT3* cRNA (*OPT3*) or water (Mock). Cu uptake was measured after 3 h. The uptake solution was supplemented with 25 µM Cu-NA (Cu-NA) or 100 µM $CuSO_4$ (Cu^{2+}, the final free Cu^{2+} activity in the uptake solution being estimated to be 35 µM as determined by GEOCHEM-EZ (Shaff et al. 2010)). Values are means ± SE. Asterisks indicate statistically significant differences (**, $P < 0.01$, using Student's *t*-test, $n = 5$ independent replicates; each replicate of the sample contained 8 to 10 oocytes). **B)** Cu concentration in the wild-type yeast strain SEY6210 and its isogenic *ctr1Δ2Δ3Δ* mutant both expressing the empty *YES3-Gate* vector (WT and *ctrΔ*, respectively) or the *ctr1Δ2Δ3Δ* mutant expressing *YES3-Gate-OPT3* (*OPT3*), grown with 20 µM $CuSO_4$. Different lowercase letters indicate significant differences ($n = 4$ to 5 independent ICP-MS measurements [independently grown cells]), ANOVA followed by Tukey's HSD test). **C)** Wild-type yeast strain SEY6210 (WT) and the *ctr1Δ2Δ3Δ* mutant transformed with the empty *YES3-Gate* vector or *ctr1Δ2Δ3Δ* transformed with the vector containing the *OPT3* cDNA (*OPT3*) or the Arabidopsis Cu transporter gene *COPT2* (*COPT2*), were diluted 10-fold serially and spotted onto solid YPEG medium supplemented with different concentrations of $CuSO_4$. Colonies were visualized after incubating plates for 3 d at 30 °C. Dilution series are indicated on the right.

membrane Cu uptake transporter genes *Ctr1* and *Ctr3* and the vacuolar membrane Cu efflux transporter gene *Ctr2* (Dancis et al. 1994; Rees et al. 2004). Due to low internal Cu, *ctr1Δctr2Δctr3Δ* mutant cells manifest a respiratory defect because of the altered activity of the Cu-dependent cytochrome *c* oxidase complex in the mitochondrial respiratory chain. This defect can be visualized by the failure of the *ctr1Δctr2Δctr3Δ* mutant to grow on non-fermentable carbon sources such as ethanol and glycerol (YPEG medium) unless Cu is supplied exogenously (Dancis et al. 1994). Indeed, *ctr1Δctr2Δctr3Δ* cells expressing the empty YES3-Gate vector accumulated 10 times less Cu than the vector-expressing wild-type (Fig. 3B). The expression of *OPT3* in mutant cells increased their Cu accumulation by 5-fold compared to the vector-expressing cells, although it did reach the level of the vector-expressing wild-type cells (Fig. 3B).

We also compared the growth of the *ctr1*Δ*ctr2*Δ*ctr3*Δ mutant and wild-type strains expressing the empty *YES3-Gate* vector and the *ctr1*Δ*ctr2*Δ*ctr3*Δ mutant transformed with *YES3-Gate* containing the *OPT3* cDNA on a medium containing the non-fermentable carbon sources ethanol and glycerol (YPEG). The *ctr1*Δ*ctr2*Δ*ctr3*Δ mutant transformed with Arabidopsis *COPT2* was used as an additional positive control (Gayomba et al. 2013). As shown previously, vector-expressing *ctr1*Δ*ctr2*Δ*ctr3*Δ cells did not grow in YPEG medium, even when the medium was supplemented with low (10 and 20 µM) concentrations of Cu, but grew well on YPEG supplemented with 100 µM $CuSO_4$ (Fig. 3C and (Gayomba et al. 2013)). Unlike *COPT2*-expressing mutant cells, *OPT3*-expressing mutant cells did not grow in YPEG medium without supplemental Cu. However, in contrast to vector-expressing *ctr1*Δ*ctr2*Δ*ctr3*Δ cells, *OPT3*-expressing cells were able to grow when 10 µM or 20 µM $CuSO_4$ was added to the medium (Fig. 3C). These results are consistent with a role for OPT3 in Cu uptake and suggest that, unlike CTR/COPTs, OPT3 might be a low-affinity Cu transporter, at least when expressed in yeast. Together, our results show that OPT3 mediates the transport of Cu ions in heterologous systems.

The *opt3* mutant is sensitive to Cu deficiency

We next tested the sensitivity of the *opt3* mutant to Cu deficiency by comparing its growth and development to the wild-type, both grown hydroponically with or without Cu supplementation (Fig. 4). As observed previously, the rosette size of the *opt3* mutant was smaller than that of the wild-type

even under control conditions (Fig. 4A) (Stacey et al. 2008; Mendoza-Cózatl et al. 2014; Zhai et al. 2014). We found that the rosette size becomes even smaller under Cu deficiency compared to control conditions; by contrast, Cu deficiency did not affect rosette size in the wild-type (Fig. 4A) early in the vegetative stage of development. The independent *opt3-2* allele exhibited a similar sensitivity to Cu deficiency in the medium as *opt3-3* (Supplemental Fig. S6A). As evidenced by the shorter root length and lower fresh weight of the *opt3* mutant, we also observed an increased sensitivity to Cu deficiency in the *opt3-3* mutant relative to wild-type in seedlings grown on solid medium containing the Cu chelator bathocuproine disulfonate (BCS) (Supplemental Fig. S6B to D). Consistent with the increased sensitivity of the *opt3* mutant to Cu deficiency and our finding that it experiences molecular symptoms of Cu deficiency, cupric reductase activity was significantly higher in roots of the *opt3* mutant than in wild-type (Supplemental Fig. S6E).

We then tested whether the transition to flowering was delayed in the *opt3* mutant under control conditions and/or under Cu deficiency, as we recently showed that Cu was involved in this developmental decision (Rahmati Ishka and Vatamaniuk 2020). Consistent with our recent findings, wild-type plants flowered significantly later and developed more rosette leaves when grown hydroponically without Cu than with Cu (Fig. 4B to D and Table 1). The *opt3* mutant failed to flower within the time frame of the experiment (8 wk) and developed 30%- and 90% more rosette leaves than the wild-type when grown on medium without or with $CuSO_4$, respectively (Fig. 4, C and D and Table 1). Leaves of the *opt3* mutant were significantly shorter and were extensively chlorotic compared to the wild-type, when both were grown without added Cu (Fig. 4, E and F). Although the length of the rosette leaves from mutant and wild-type plants was comparable to control Cu levels (125 nM $CuSO_4$), the leaves of the mutant possessed Cu-deficiency-characteristic chlorotic spots (Fig. 4F). The delayed transition to flowering, the increased number, and the length of rosette leaves of the mutant were rescued by transferring the mutant to medium with high (500 nM) $CuSO_4$ (Fig. 4C to E, Table 1 and Supplemental Fig. S7A). Transferring the mutant to a lower (250 nM) Cu concentration also rescued the small size of the mutant, although to a lesser extent compared to the higher Cu concentration (500 nM) (Supplemental Fig. S7B).

The *opt3* mutant mounts transcriptional Fe-deficiency responses in roots but not in shoots

We next used transcriptome deep sequencing (RNA-seq) to test whether the expression of Cu deficiency-responsive genes was altered in roots, mature and young leaves of the *opt3* mutant compared to the wild-type. Using Illumina sequencing, we obtained 54, 79, and 59 million clean reads from roots, mature and young leaves, respectively (Supplemental Data Set S1). Of these, 86% of reads from roots and mature leaves and 93% of reads from young leaves mapped to the Arabidopsis reference genome and were employed to estimate transcript abundance and differential expression. Compared to wild-type, we identified 376, 673, and 1,942 differentially expressed genes (DEGs) in *opt3* mutant roots, young leaves and mature leaves, respectively (ratio $\geq$ 1.5 or $\leq$ 0.67, false discovery rate [FDR] $<$ 0.05; Fig. 5, A to C). We confirmed the higher expression of canonical Fe deficiency-responsive genes, known to positively regulate Fe-deficiency responses to facilitate Fe uptake (*FIT*, *IRT1*, *FRO2*, *bHLH38*, *bHLH39*, *bHLH100*, *bHLH101*, *MYB10*, *MYB72*), the Fe-sensing peptide gene *FEP2/IMA2*, coumarin biosynthesis, and transport genes (*CYP82C4*, *S8H* and *PDR9/ABCG37*) in *opt3* mutant roots (Fig. 5B and Supplemental Data Set S2). In addition, we detected IRT1 in the roots of the *opt3* mutant grown under control conditions and the roots of the wild-type grown under Fe deficiency but not in the roots of the wild-type or the *fit-2* mutant grown under control conditions by immunoblot analysis (Supplemental Fig. S8). Of other Fe deficiency-regulated genes, *FRO3*, encoding a chloroplast-localized protein, and the Fe exporter gene *FE REGULATED 3* (*IREG3*, also named *FERROPORTIN 3* [*FPN3*]), whose encoded protein is dual-targeted to mitochondria and chloroplasts, were also upregulated in *opt3* mutant roots compared to the wild-type (Fig. 5B and Supplemental Data Set S2). Of 237 genes upregulated in *opt3* mutant roots, 32 (or 13.5%) were among robust FIT targets, and six (or 0.025%) were among POPEYE (PYE) targets (Supplemental Data Set S2 and (Mai et al. 2015)), suggesting that the *opt3* mutant mounts a primarily FIT-regulated Fe deficiency response under Fe-sufficient conditions.

Notably, the expression of a negative FIT regulator gene, *ZAT12*, was upregulated in roots of the *opt3* mutant vs. wild-type as well (Fig. 5B and Supplemental Data Set S2). In addition, the expression of genes mediating cellular response to Fe overload was upregulated. Specifically, the expression of *FER1* encoding a chloroplast-localized Fe-sequestering protein, whose expression is upregulated by Fe overload to protect chloroplasts from Fe toxicity, was upregulated in the roots of the *opt3* mutant compared to the wild-type (Fig. 5B and Supplemental Data Set S2). The expression of *IREG2/FPN2*, *VTL1*, *VTL2*, and *VTL5* mediating Fe sequestration into the vacuole was upregulated as well (Fig. 5B and Supplemental Data Set S2). These data suggest that despite the upregulated FIT-transcriptional network, root cells also perceived the Fe-sufficiency/overload signal and responded by increasing the expression of FIT negative regulators and genes involved in mitigating Fe-overload toxicity.

It is noteworthy that while *opt3* mutant roots constitutively overexpressed genes encoding Fe uptake components even when grown in Fe-sufficient conditions, the magnitude of the response was considerably larger when the mutant was grown under Fe deficiency (Fig. 5D). This result was consistent with the important role of OPT3 in mitigating and controlling the basal response of the root to Fe deficiency.

We then compared the expression of Fe-deficiency responsive genes in young and mature leaves of the *opt3*

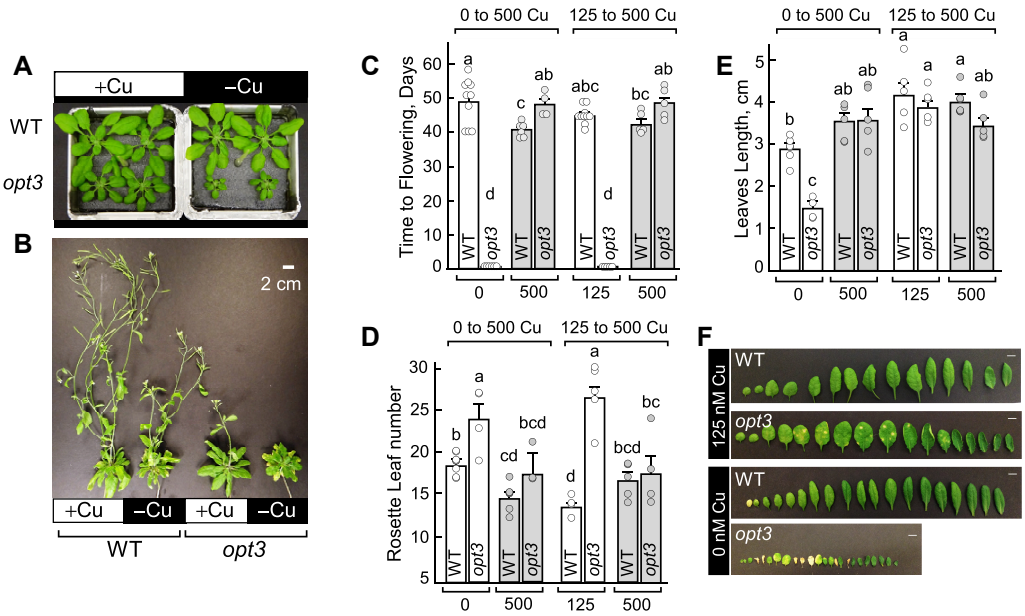

Figure 4. The *opt3-3* mutant Is sensitive to Cu deficiency. **A** and **B)**, wild-type (WT) and the *opt3-3* mutant (*opt3*) were grown hydroponically with (+ Cu) or without (− Cu) 125 nM $CuSO_4$. Images were taken 4 wk **A)** or 9 wk **B)** from seed sowing. Data for the *opt3-2* allele and wild-type are shown in Supplemental Figure S6A. **C-E)** Time to flowering **C)**, primary rosette leaf number **D)** and leaf length **E)**. Seeds were germinated and plants grown hydroponically without or with Cu (0 or 125, respectively and white bars). After 4 wk of growth, a subset of plants grown with or without Cu was transferred to 500 nM $CuSO_4$ (500 and gray bars). Measurements were taken after the appearance of the first flower. A and B show a representative image of plants from three independently conducted experiments. In C-D, values are means ± SE. Different lowercase letters indicate significant differences (ANOVA followed by Tukey's HSD, JMP Pro 14 software package). Data were combined from three ($n = 3$ for *opt3*) to five ($n = 5$ for wild-type) independent experiments. In each independent experiment, measurements were taken from two plants per genotype and per condition. **F)** shows a representative image of leaves (from young to old in the direction from left to right) of the wild-type and the *opt3-3* mutant both grown hydroponically for 4 wk without (0 nM Cu) or with Cu (125 nM Cu).

Table 1. Average day from the date of sowing to flowering in wild-type and the *opt3-3* mutant grown hydroponically with 0 or 125 nM $CuSO_4$A subset of plants was shifted to 500 nM Cu[a]

	Cu concentrations, nM			
Genotype	0	0 to 500	125	125 to 500
Wild-type (Col-0)	46.8 ± 2.9	40.2 ± 0.8	42.3 ± 0.8	41.8 ± 1.2
opt3-3	N.A.[b]	48.0 ± 1.8	N.A.[b]	48.4 ± 1.8

[a]Values are means ± standard error ($n = 3$ to 6).
[b]N.A.; not applicable. The mutant did not flower during the course of measurements, which ranged from 5 to 8 wk.

mutant and wild-type. Unlike roots, both mature and young leaves of the *opt3* mutant did not show a transcriptional Fe deficiency response. Specifically, none of the canonical Fe-deficiency upregulated genes were upregulated in young or mature leaves of the *opt3* mutant (Fig. 5B and Supplemental Data Sets S3 and S4). Moreover, *FEP1/IMA3*, known to be involved in Fe sensing and typically upregulated in leaves and roots under Fe deficiency (Grillet et al. 2018), was downregulated in mature leaves of the *opt3* mutant relative to the wild-type; At5g05250, encoding a protein of unknown function and upregulated by Fe deficiency in leaves of different Arabidopsis accessions (Waters et al. 2012), was downregulated in both young and mature leaves of the *opt3* mutant compared to the wild-type. Fe deficiency-downregulated genes *NICOTIANAMINE SYNTHASE 3* (*NAS3*), *YELLOW STRIPE-LIKE 1* (*YSL1*) and *YSL3* were highly upregulated in mature leaves in the *opt3* mutant, and *YSL1* was also upregulated in young leaves of the *opt3* mutant compared to the wild-type (Fig. 5B and Supplemental Data Sets S3 and S4). *FRO7*, encoding a chloroplast-localized ferric chelate reductase, as well as *FRO6*, encoding a plasma membrane-localized protein, were highly upregulated in mature leaves of the *opt3* mutant relative to wild-type, although their expression is not regulated by Fe deficiency in Arabidopsis shoots (Mukherjee et al. 2006) (Fig. 5B and Supplemental Data Set S3). We also observed the high upregulation of Fe-sufficiency markers *FER1*, *FER3*, and *FER4* in both mature and young leaves of the *opt3* mutant compared to the wild-type (Fig. 5B and Supplemental Data Sets S3 and S4). Together, our RNA-seq data help unravel the details of contrasting responses of the Fe regulon in roots, young and mature leaves of the *opt3* mutant and support the past observation that *opt3* mutant leaves sense Fe overload (Khan et al. 2018).

The *opt3* mutant mounts a transcriptional Cu deficiency response

Roots of the *opt3* mutant accumulated significantly less Cu than the roots of wild-type plants, albeit total internal Cu

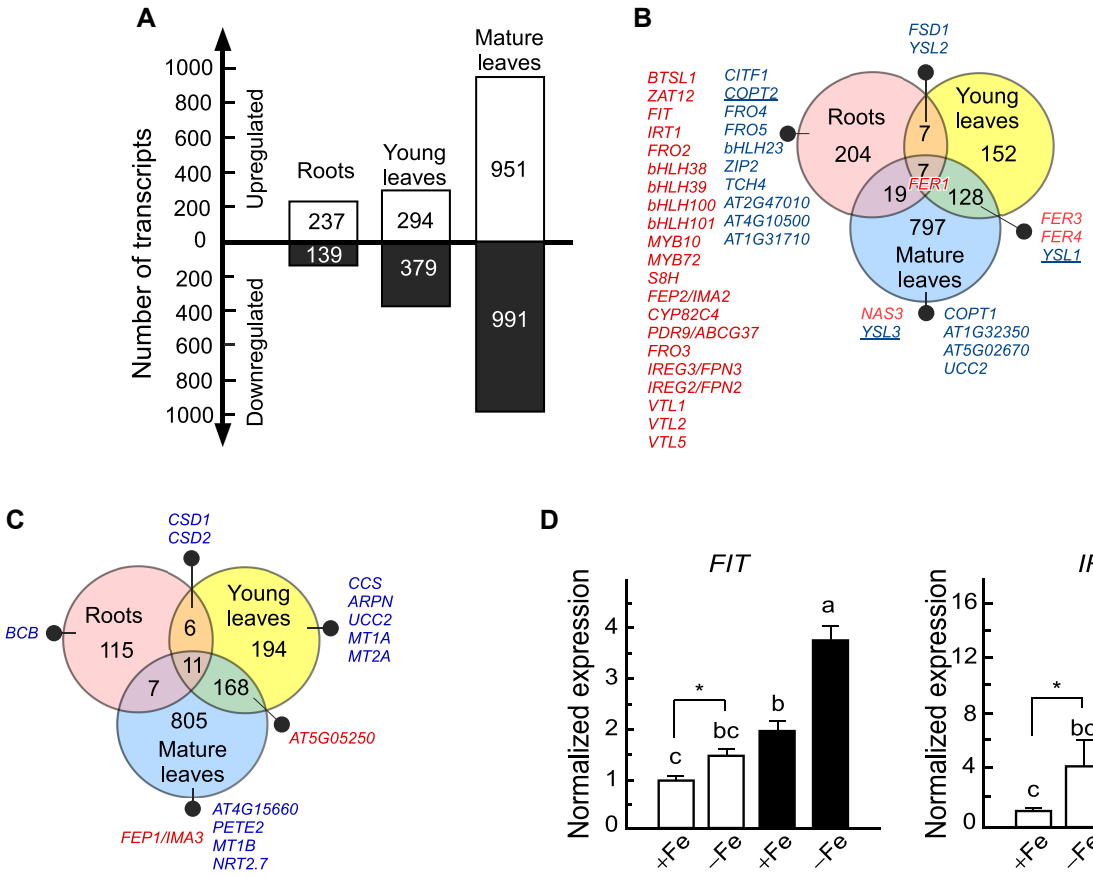

Figure 5. The *opt3-3* mutant mounts a Cu deficiency response in roots and young leaves. **A)** Total number of differentially expressed genes in roots, mature leaves and young leaves of the *opt3* mutant compared to wild-type, according to RNA-seq data (ratio >= 1.5 or <=0.67, false-discovery rate [FDR] < 0.05). **B, C)** Venn diagrams showing the number of upregulated **B)** or downregulated **C)** genes in roots, mature and young leaves. Overlaps indicate the number of genes co-regulated in the indicated tissues. Genes associated with Fe and Cu homeostasis are shown in **B)** and **C)**. Genes involved in Cu homeostasis are marked in bold; genes associated with Fe and Cu deficiency responses are marked in bold and are underlined. **D)** The expression of the Fe transport system is upregulated in the roots of the *opt3* mutant under Fe deficiency. Plants were grown hydroponically for 31 d. A subset of plants sas transferred to fresh medium with no added Fe. Roots were collected after 4 d of additional growth with or without Fe. White and black bars represent the transcript abundance of the indicated genes in the wild-type and the *opt3* mutant, respectively. Values are means ± SE. ($n = 3$ independent RT-qPCR experiments per genotype. In each experiment, roots were pooled from four plants grown in the same container for RNA extraction). Asterisks indicate statistically significant differences in gene expression in wild-type grown with or without Fe ($P < 0.05$, Student's *t*-test). Different lowercase letters indicate significant differences ($P < 0.05$; ANOVA followed by Tukey HSD, JMP Pro 14 software package).

concentration in the mutant roots reached what would be considered sufficiency (Fig. 2A and (Broadley et al. 2012)). We therefore anticipated that the expression of genes belonging to the Cu-deficiency regulon in roots would not be altered in the *opt3* mutant. However, we discovered that the expression of canonical Cu-deficiency induced genes responsible for Cu uptake (*CITF1*, *COPT2*, *FRO4*, and *FRO5*) is upregulated in *opt3* mutant roots compared to wild-type roots (Table 2, Fig. 5B and Supplemental Data Set S2).

Since small RNAs were not included in the RNA-seq analysis, we tested the expression of canonical Cu *MIRNA* precursors in roots of the *opt3* mutant and wild-type plants by RT-qPCR (Pilon 2017). The precursors *MIR397a/b*, *MIR857a*, *MIR389b/c*, and *MIR408* were upregulated in *opt3* roots when compared to wild-type roots (Fig. 6A). Moreover, the Cu deficiency-repressed genes *Cu/Zn SUPEROXIDE DISMUTASE 1* (*CSD1*), *CSD2* and *BLUE-CU-BINDING PROTEIN* (*BCB*), contributing to Cu economy/metal switch, were downregulated by more than 2-fold. Consistently, the expression of *FSD1* (*FE SUPEROXIDE DISMUTASE 1*) was upregulated by 2.7-fold in roots of the *opt3* mutant compared to the wild-type (Table 2, Fig. 5C and Supplemental Data Set S2). In addition, several other canonical Cu-deficiency upregulated genes (*bHLH23*, *ZRT/IRT-LIKE PROTEIN 2* [*ZIP2*], *YSL2*, *TOUCH 4* [*TCH4*], At2g47010, At4g10500, At1g31710, (Bernal et al. 2012; Waters et al. 2012, 2014; Yan et al. 2017; Schulten et al. 2022)) were upregulated in roots of the *opt3* mutant compared to the wild-type (Table 2, Fig. 5B and Supplemental Data Set S2). Of 16 Cu-deficiency regulated genes in the *opt3* mutant, 10 are considered to be SPL7-dependent (Supplemental Data Set S2). These results

Table 2. Expression of Cu deficiency-responsive genes in roots, mature leaves and young leaves of the *opt3-3* mutant. Wild-type Arabidopsis and *opt3-3* plants were grown hydroponically with 0.125 μM $CuSO_4$ for 4 wk prior to tissue collection for RNA-seq analysis. Upregulated or downregulated genes are shown in bold font and marked with asterisks (ratio >= 1.5 or <=0.67, [FDR] < 0.05)

AGI ID	Gene Name	RPKM[a]						Ratio (*YL* vs *ML*[b])				
		*opt3*_R[b]	wt_R[b]	*opt3*_ML[b]	wt_ML[b]	*opt3*_YL[b]	wt_YL[b]	R[b]	ML[b]	YL[b]	wt	*opt3*
AT5G59030	*COPT1*	7.3	3.5	164.4	98.9	68.3	60.4	2.1	**1.7**[a]	1.1	**0.6**[a]	**0.4**[a]
AT3G46900	*COPT2*	183.3	46.1	1.6	2.0	0.4	0.1	**4.0**[a]	0.8	3.3	**0.1**[a]	**0.2**[a]
AT2G26975	*COPT6*	0.3	0.3	38.2	26.1	16.5	17.7	1.1	1.5	0.9	0.7[a]	**0.4**[a]
AT4G24120	*YSL1*	0.2	0.4	10.4	3.3	4.3	2.5	0.4	**3.1**[a]	**1.7**[a]	0.8	**0.4**[a]
AT5G24380	*YSL2*	19.2	10.3	1.5	1.0	1.3	0.5	**1.9**[a]	0.7	**2.8**[a]	**0.5**[a]	0.9
AT5G53550	*YSL3*	19.3	20.5	21.0	11.6	8.2	8.6	0.9	**1.8**[a]	1.0	0.7[a]	**0.4**[a]
AT5G23980	*FRO4*	221.4	103.4	5.6	8.7	0.6	0.8	**2.1**[a]	0.7	0.7	**0.1**[a]	**0.1**[a]
AT5G23990	*FRO5*	326.7	39.5	0.5	0.7	0.1	0.0	**8.3**[a]	0.8	NA	**0.2**[a]	**0.1**[a]
AT1G71200	*CITF1*	9.6	1.5	0.0	0.0	0.0	0.0	**6.6**[a]	NA	NA	1.0	0.3
AT1G08830	*CSD1*	100.0	243.4	69.3	102.0	28.2	181.1	**0.4**[a]	0.7	**0.2**[a]	1.8	**0.4**[a]
AT2G28190	*CSD2*	72.7	123.3	68.8	151.0	138.6	452.8	**0.6**[a]	0.5	**0.3**[a]	**3.0**[a]	2.0
AT2G02850	*ARPN*	17.9	19.6	0.7	0.7	2.2	6.5	0.9	1.0	**0.3**[a]	**9.8**[a]	**3.3**[a]
AT5G20230	*BCB*	1.4	3.6	258.6	325.8	41.3	110.8	**0.4**[a]	0.8	0.4	**0.3**[a]	**0.2**[a]
AT1G12520	*CCS1*	32.7	55.8	18.6	20.9	12.5	39.4	**0.6**[a]	0.9	**0.3**[a]	1.9	**0.7**[a]
AT2G44790	*UCC2*	1068.8	1418.9	4.5	1.9	1.3	4.4	**0.8**[a]	**2.4**[a]	**0.3**[a]	2.3	**0.3**[a]
AT4G25100	*FSD1*	332.0	120.9	807.2	584.7	681.3	264.0	**2.7***	1.4	**2.6***	**0.5***	0.8*
AT3G56240	*CCH*	243.0	171.8	103.8	96.9	42.6	39.8	**1.4**[a]	1.1	1.1	**0.4**[a]	**0.4**[a]
AT1G71040	*LPR2*	30.1	31.0	102.9	83.5	35.6	43.3	1.0	1.2	0.8	**0.5**[a]	**0.4**[a]
AT2G07687	*COX3*	1.1	2.3	1.0	1.3	0.3	0.7	0.5	0.8	0.4	0.5	**0.3***
AT1G18140	*LAC1*	2.4	2.9	0.0	0.0	0.4	1.0	0.8	NA	0.4	**98.0***	**14.6***
AT2G29130	*LAC2*	22.4	28.3	0.1	0.3	0.4	1.0	0.8	0.2	0.5	3.2	**7.4**[a]
AT2G46570	*LAC6*	2.6	2.6	0.7	0.4	3.2	3.2	1.0	1.8	1.0	**8.2**[a]	**4.6**[a]
AT5G01600	*FER1*	286.9	167.6	1349.9	97.8	642.6	112.6	**1.7**[a]	**13.8**[a]	**5.7**[a]	1.2	**0.5**[a]
AT3G56090	*FER3*	28.0	21.8	115.2	13.2	197.7	58.6	1.3	**8.7**[a]	**3.4***	**4.4**[a]	**1.7**[a]
AT2G40300	*FER4*	10.7	10.7	97.2	40.3	139.3	90.6	1.0	**2.4**[a]	**1.5**[a]	**2.3**[a]	1.4

[a]RPKM, Reads Per Kilobase of transcript per Million mapped reads.
[b]R, roots; ML, mature leaves, YL, young leaves.

show that roots of the *opt3* mutant manifest molecular symptoms of Cu deficiency, even though these plants were grown under Cu-sufficient conditions and the internal concentration of Cu in roots was at the level of sufficiency (Fig. 2A and Supplemental Fig. S3).

We also found that young leaves of the *opt3* mutant manifested molecular symptoms of Cu deficiency, as evidenced by the increased expression of *YSL1* and *YSL2*, which are typically upregulated under Cu deficiency and involved in lateral movement of minerals, including Cu (Fig. 5, B and C and Table 2, Supplemental Data Set S3). Genes associated with either Cu buffering (*METALLOTHIONEIN 1A [MT1A]* and *METALLOTHIONEIN 2A MT2A*) or Cu economy (*CSD1*, *CSD2*, *COPPER CHAPERONE FOR SOD1 [CCS1]*, *PLANTACYANIN [ARPN]*, *UCLACYANIN 2 [UCC2]*) were downregulated, while *FSD1* was upregulated (Fig. 5, B and C and Supplemental Data Set S3).

Turning to mature leaves, we detected a different set of genes as being differentially expressed in the *opt3* mutant compared to the wild-type, and the pattern of the regulation (up or down) of canonical Cu-deficiency-regulated genes was not symptomatic for either deficiency or sufficiency (Supplemental Data Set S4). Specifically, as might be expected under Cu deficiency, the expression of the genes *COPT1*, *YSL1*, and *YSL3*, which are associated with Cu uptake and lateral movement, was higher in the *opt3* mutant than in wild-type. Other Arabidopsis Cu-deficiency upregulated genes, including At1g32350 and At5g02670, were also upregulated in mature leaves of the *opt3* mutant. Of genes typically downregulated by Cu deficiency, At4g15660 was also downregulated in the *opt3* mutant relative to the wild-type, as well as *PLASTOCYANIN 2 (PETE2)*, associated with Cu sparing, and *METALLOTHIONEIN 1B (MT1B)*, associated with Cu buffering. By contrast, the expression of another Cu sink, *UCC2*, which is typically downregulated by Cu deficiency, was upregulated in mature leaves of the *opt3* mutant compared to the wild-type, while *NITRATE TRANSPORTER 2.7* (*NRT2.7*), typically upregulated by Cu deficiency in Arabidopsis, was downregulated in the *opt3* mutant.

To conclude, our RNA-seq data show that both roots and young leaves of the *opt3* mutant mounted a transcriptional Cu deficiency response while only mutant roots manifested a transcriptional Fe-deficiency response. In addition, our finding of the distinct transcriptional response and metal accumulation between mature and young leaves of the mutant emphasizes the need to separate these leaves in analyses of mutant phenotypes.

OPT3 is transcriptionally upregulated by short-term Cu deficiency

While *OPT3* is robustly upregulated in roots and leaves by Fe deficiency, it was not among Cu deficiency-responsive

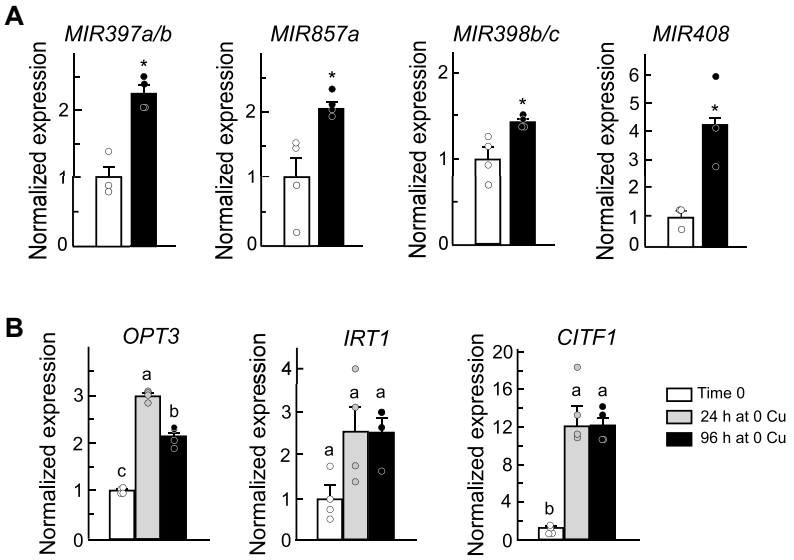

Figure 6. The expression of Cu *MIRNA* genes is upregulated in the *opt3-3* mutant. **A)** Transcript abundance of *MIRNA397a/b*, *MIR857a*, *MIR398b/c*, and *MIR408* precursors in roots of 5-wk-old wild-type (open bars) or the *opt3* mutant (black bars) grown hydroponically with 125 nM $CuSO_4$. Values are means ± SE. Asterisks indicate significant differences compared to wild-type, which was set to 1 ($P < 0.05$, Student's *t*-test, $n = 4$ independent RT-qPCR experiments per genotype. In each experiment, roots were pooled from four plants grown in the same container for RNA extraction). **B)** Relative expression levels of *OPT3*, *IRT1* and *CITF1* in roots of wild-type subjected to 1 to 4 d of Cu deficiency. *CITF1* was used as a marker of Cu deficiency to validate treatment efficiency. Values are means ± SE. Different lowercase letters indicate significant differences ($P < 0.05$; ANOVA followed by Tukey's HSD, JMP Pro 14 software package, $n = 4$ independent RT-qPCR experiments per condition. In each experiment, roots were pooled from four plants grown in the same container for RNA extraction.

genes in existing RNA-seq datasets. In these previous RNA-seq analyses, plants were exposed to Cu deficiency for a minimum of 3 d. Since *OPT3* responds to Fe deficiency within 24 h (Khan et al. 2018), we hypothesized that *OPT3* might also be transcriptionally upregulated by short-term exposure to Cu deficiency. Thus, we compared *OPT3* expression in Arabidopsis subjected to Cu deficiency for 24 or 96 h. We also examined the expression of the Cu-deficiency marker *CITF1* to validate the efficiency of our treatments. *CITF1* was upregulated in roots 16-fold after 24 h of Cu deficiency and remained highly upregulated after 96 h. The expression of *OPT3* was also upregulated, although to a lesser extent, after 24 h of Cu deficiency, but unlike *CITF1*, the transcript abundance of *OPT3* decreased after 96 h of treatment (Fig. 6B). *IRT1* expression was not upregulated by Cu deficiency (Fig. 6B).

Supplemental Cu rescues the molecular symptoms of Cu deficiency in the *opt3* mutant

Since transferring the *opt3* mutant to higher Cu concentrations decreased its time to flowering to the level of wild-type and rescued the length of rosette leaves (Fig. 4 and Supplemental Fig. S7A), we predicted that supplemental Cu would also decrease the expression of Cu deficiency-responsive genes. To test this hypothesis, we compared the transcript levels of the Cu deficiency markers *CITF1*, *COPT2*, *FRO4*, and *FRO5* in the roots of the *opt3* and wild-type. In parallel, we also tested the expression of the key Fe deficiency markers *IRT1* and *FRO2*. Consistent with the RNA-seq data (Table 2), the expression of *CITF1*, *COPT2*, *FRO4*, and *FRO5* was upregulated in roots of the *opt3* mutant relative to the wild-type, which were both grown under control conditions (Fig. 7). The transcript levels of Cu deficiency markers dropped in *opt3* mutant roots after transfer to higher Cu concentrations (Fig. 7A to H). We note that transferring wild-type plants to higher Cu also decreased the expression levels of *CITF1*, *COPT2*, *FRO4*, and *FRO5*, suggesting that 125 nM $CuSO_4$ was somewhat Cu-limiting, even though the growth and development of wild-type plants were not affected. Supplemental Cu in both concentrations also decreased the expression levels of *IRT1* and *FRO2* in *opt3* mutant roots compared to their levels under control conditions (Fig. 7, J to M). It is worth noting that the higher Cu concentration (500 nM) increased the expression of both *IRT1* and *FRO2* in wild-type roots, reinforcing the existence of interactions between Cu and Fe homeostasis.

OPT3 function in the shoot regulates both Fe and Cu deficiency responses of the root

We next tested whether the increased expression of Cu deficiency markers in *opt3* mutant roots was due to its altered shoot-to-root signaling. To this end, we used reciprocal grafting with wild-type and *opt3* plants and examined the transcript levels of the Cu-deficiency markers *CITF1*, *COPT2*, *FRO4*, *FRO5* in roots (Fig. 8). Their expression was upregulated in the roots of grafted *opt3*/*opt3* (*opt3* scions grafted to *opt3*

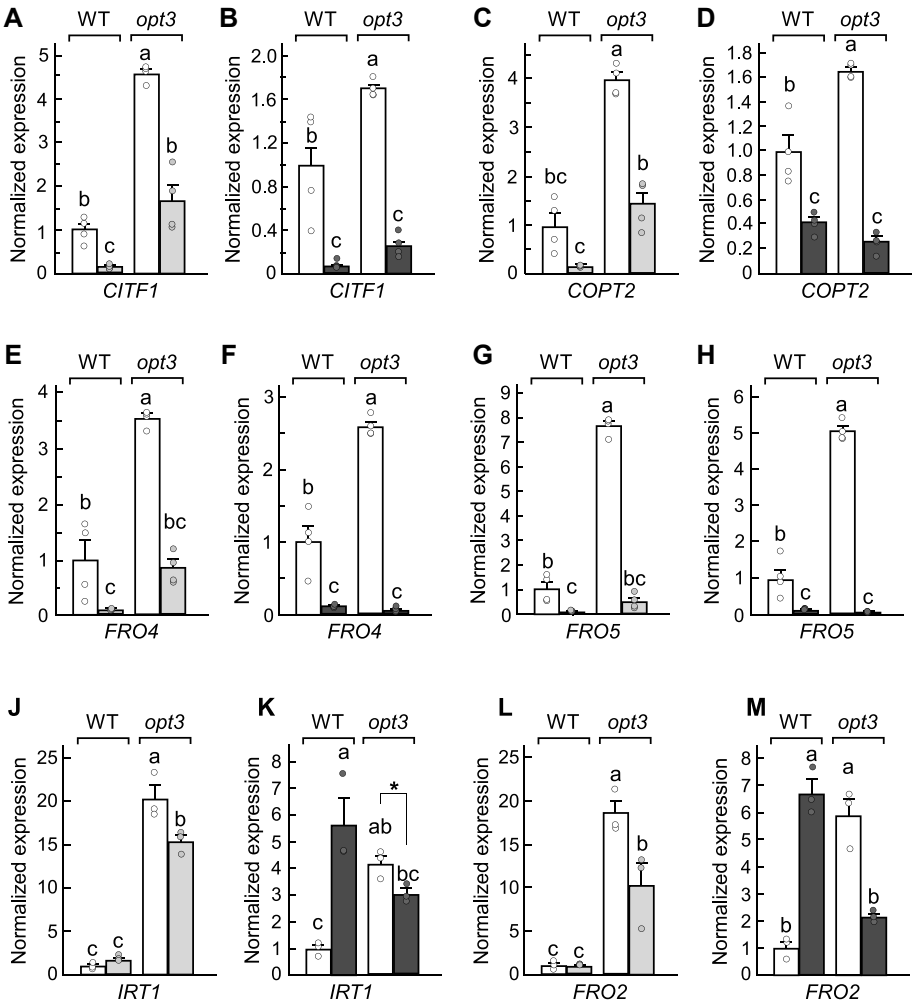

Figure 7. Cu supplementation partially rescues the molecular symptoms of Cu deficiency in *opt3-3* mutant roots. Plants were grown hydroponically under control conditions (white bars) until the late-vegetative stage before a subset of plants was transferred to fresh medium with higher Cu concentrations (250 nM $CuSO_4$, light gray bars in **A, B, E, F, J, K** or 500 nM $CuSO_4$, dark gray bars in **C, D, G, H, L, M**). Plants were grown for another week before tissue collection and RT-qPCR analysis. The transcript abundance of the indicated genes was normalized to the wild-type grown under control conditions. Values are means ± SE. Different lowercase letters indicate significant differences (ANOVA followed by Tukey's HSD, JMP Pro 14 software package, $n = 3$ RT-qPCR experiments per genotype). In each experiment, roots were pooled from three plants grown in one container for RNA extraction. Data are normalized to the expression of *ACTIN2*; the expression of genes in the wild-type grown under 125 nM $CuSO_4$ (control conditions) was set to one.

rootstocks) compared to grafted WT/WT (wild-type [WT] scions grafted to WT rootstocks [control grafts], Fig. 8A). The expression of *CITF1*, *COPT2*, *FRO4*, and *FRO5* was also elevated in roots of grafts with *opt3* scions and wild-type rootstock (Fig. 8A). By contrast, grafting of wild-type shoots onto *opt3* rootstocks downregulated *CITF1*, *COPT2*, *FRO4*, and *FRO5* expression relative to control grafts (Fig. 8A). These data show that OPT3 function in the shoot is sufficient to regulate the transcriptional Cu deficiency responses in the root.

Grafted plants performed as expected, as evidenced by the expression of the Fe-deficiency markers *IRT1* and *FRO2* in different graft combinations (Fig. 8B and (Zhai et al. 2014)). As shown previously, *IRT1* and *FRO2* were upregulated in roots of *opt3*/*opt3* compared to WT/WT grafts (Fig. 8B and (Zhai et al. 2014)). Grafting wild-type shoots onto *opt3* mutant roots downregulated *IRT1* and *FRO2* expression relative to their expression in control grafts (Fig. 8B). By contrast, grafting of *opt3* shoots onto wild-type roots increased the expression of Fe deficiency markers (Fig. 8B). Together, these data show that OPT3 function in the shoot regulates both Fe- and Cu-deficiency responses of the root. These data also suggest the existence of systemic shoot-to-root Cu status signaling.

Cu feeding *via* the phloem in the shoot regulates the expression of Cu- and Fe-deficiency responsive genes in roots

To test whether the Cu status of the shoot can be communicated to the root and whether Cu movement *via* the

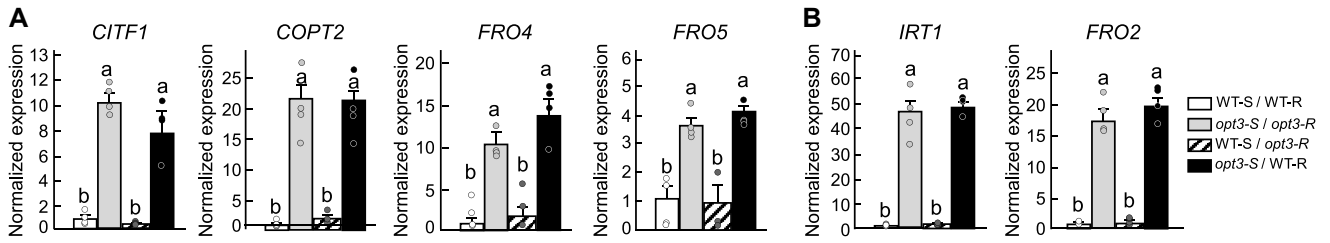

Figure 8. The OPT3 function in the shoot controls the expression of Cu deficiency markers. Transcript abundance of Cu- **A)** and Fe-deficiency **B)** markers in the roots of grafted plants. The wild-type and the *opt3-3* mutant were used for reciprocal grafting. WT-S/WT-R, wild-type scion grafted to wild-type rootstock (control); *opt3*-S/*opt3*-R, *opt3* scion grafted to *opt3* rootstock; WT-S/*opt3*-R, wild-type scion grafted to *opt3* rootstock; *opt3*-S/WT-R, *opt3* scion grafted to wild-type rootstock. Values are means ± SE. ($n = 4$ independent experiments [PCR runs, each representing an independent experimental setup]; roots were pooled from four plants per the experimental setup). Different lowercase letters indicate significant differences ($P < 0.05$; ANOVA followed by Tukey's HSD, JMP Pro 14 software package). Data were normalized to the expression of *ACTIN2*; the expression of genes in the wild-type was set to one.

phloem from the shoot to the root influences the expression of Cu acquisition genes, we performed phloem-feeding experiments via the abrasion of the leaf vasculature. We first tested this approach using the phloem symplastic tracer 5,6 carboxyfluorescein-diacetate (CFDA) (Grignon et al. 1989; Oparka et al. 1994). After diffusing into plant cells, CFDA is cleaved by cellular esterases to yield a membrane-impermeable form of the dye carboxyfluorescein (CF). Indeed, we detected CF accumulation in the roots of wild-type plants after CFDA solution feeding via an incision in the leaf vasculature (Supplemental Figure S9, A and B).

Since systemic signaling of Fe deficiency has already been established, we first exposed wild-type Arabidopsis plants to Fe deficiency and assessed whether Fe feeding to the phloem in the shoot would rescue the expression of the Fe deficiency markers *FIT* and *IRT1*. Since *COPT2* is also upregulated by Fe deficiency via *FIT*, we used *COPT2* as a marker for Fe as well as Cu deficiency. We also used *CITF1* because of its contrasting response to Fe and Cu deficiencies: downregulated by Fe deficiency and upregulated by Cu deficiency (Yan et al. 2017). Consistent with one of the proposed roles of Fe in systemic signaling, feeding Fe via the phloem in the shoot of Fe-deficient plants decreased the expression of *FIT*, *IRT1*, and *COPT2*, while increasing *CITF1* expression (Fig. 9A). We also noticed that Fe, but not mock-feeding, rescues the chlorosis of young leaves from Fe-deficient plants (Supplemental Fig. S9D). These data are consistent with the proposed regulatory role of Fe availability in the phloem in the shoot in controlling the expression of Fe-deficiency responsive genes in the root. Some of these genes (*COPT2* and *CITF1*) also respond to Cu deficiency.

We then exposed wild-type to Cu deficiency, fed Cu to the vasculature in the shoot and determined that the expression of the Cu-deficiency markers *CITF1*, *COPT2* and Cu miRNAs precursors, *MIR397a/b*, *MIR857a*, *MIR389a/b*, and *MIR408* is significantly downregulated in the root (Fig. 9B). Interestingly, we also found that Cu feeding via the phloem in the shoot downregulates *FIT* and *IRT1* expression (Fig. 9B). These data show that Cu availability in the phloem in the shoot can influence the expression of not only Cu but also Fe deficiency-responsive genes in the root.

Feeding Cu or Fe to the phloem in the shoot of the *opt3* mutant attenuates the expression of both Fe and Cu deficiency-responsive genes in *opt3* mutant roots

Past studies of foliar Fe application by Fe spraying did not rescue the expression of Fe acquisition genes, which are constitutively overexpressed in *opt3* mutant roots (Garcia et al. 2013). This finding is not surprising considering the defect exhibited by the *opt3* mutant in Fe and Cu loading to the phloem in leaves (Figs. 1, F, G, K and 5B and (Zhai et al. 2014)). We thus asked whether feeding with Fe via the vasculature in the shoot would rescue the expression of the Fe-deficiency markers *FIT* and *IRT1* in the root. Consistent with the suggested repressive role of Fe in the phloem, the expression of *FIT* and *IRT1* was downregulated in roots of Fe-fed plants compared to mock-fed plants (Fig. 9C). Unexpectedly, we also found that the expression of the Cu deficiency markers *CITF1* and *COPT2* is downregulated in the root of the Fe-fed mutant relative to the mock-fed mutant (Fig. 9C). Interestingly, the expression of *MIR397a/b*, *MIR857a*, *MIR389a/b*, and *MIR408* precursors in the *opt3* mutant root did not respond to the phloem-feeding with Fe in the shoot (Fig. 9C).

Next, we fed Cu to the phloem in the shoot to test whether it would have a similar repressive effect on the expression of Fe- and Cu-deficiency-regulated genes in *opt3* mutant roots. The expression of Cu-deficiency markers, including *CITF1*, *COPT2* and *MIR397a/b*, *MIR857a*, *MIR389a/b*, and *MIR408* precursors, was significantly downregulated in the roots of Cu-fed compared to the mock-fed mutant (Fig. 9D). The expression of the Fe-deficiency marker genes *FIT* and *IRT1*, which are constitutively upregulated in the *opt3* mutant, was also downregulated in *opt3* mutant roots compared to the mock-fed mutant (Fig. 9D). Together, these data suggest the existence of crosstalk between Fe and Cu in shoot-to-root systemic signaling directed at the regulation of Cu and Fe uptake system in the root.

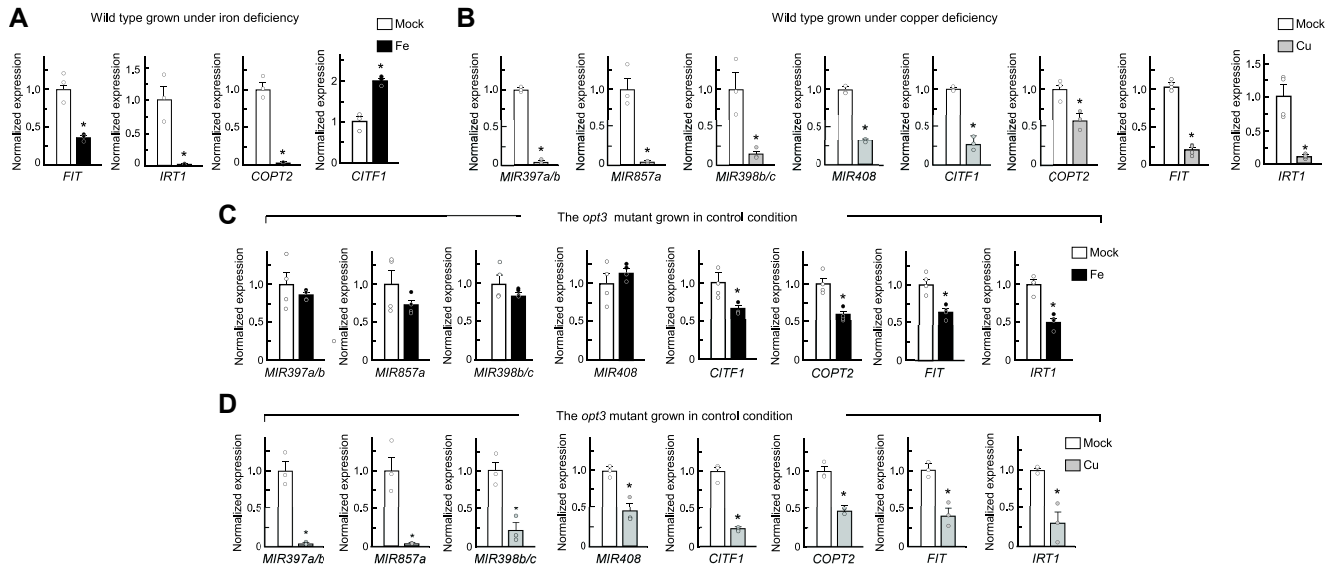

Figure 9. Cu or Fe feeding via the phloem in the shoot represses the molecular symptoms of Cu and Fe deficiencies in the root of the wild-type and the *opt3-3* mutant. RT-qPCR analysis of Cu- and Fe-deficiency molecular markers in the roots of 33-day-old wild-type **A, B)** or the *opt3* mutant **C, D)**. Wild-type plants were grown hydroponically and subjected to either Fe **A)** or Cu **B)** deficiency. The *opt3* mutant was grown hydroponically in Cu- and Fe-sufficient conditions (C, D). Roots were collected after 24 h of phloem-feeding with Fe (black bars) or Cu (gray bars) or control feeding (mock, open bars). The mock treatment for Cu feeding was MiliQ water, and the mock treatment for Fe feeding was citrate. Asterisks indicate statistically significant differences from the expression of genes in mock-fed plants, set to one ($P < 0.05$, Student's *t*-test, $n = 4$ [PCR runs, each representing an independent experimental setup]; roots were pooled from four plants per each experimental setup). Data are normalized to the expression of *ACTIN2*; the expression of genes in mock-treated wild-type (A, B) or mock-treated *opt3* (C, D) was set to one.

Cu or Fe feeding via the phloem downregulates the expression of *CITF1*, *Cu MIRNA* precursors and *FIT* in Arabidopsis roots subjected to simultaneous Cu and Fe deficiencies.

We showed that Cu and Fe accumulation in the phloem was lower in the *opt3* mutant than in the wild-type and that OPT3 function is important for regulating Cu- and Fe-deficiency responses in the root (Figs. 1, 8 and 9). To mimic the effect of simultaneous Cu and Fe deficiencies in the phloem of the *opt3* mutant and explore its influence on the expression of corresponding deficiency markers in roots, we subjected wild-type Arabidopsis plants to concurrent Fe and Cu deficiencies. We tested the expression of *CITF1* and *MIR397a/b*, *MIR857a*, *MIR389a/b*, and *MIR408* precursors because these genes are highly regulated by Cu deficiency and are downregulated by Fe deficiency (Waters et al. 2012; Yan et al. 2017). We also tested *FIT* expression, as it is responsive to Fe but not Cu deficiency (Colangelo and Guerinot 2004; Bernal et al. 2012). We determined that Cu and Fe deficiencies applied individually have an opposite effect on the expression of *CITF1* and *MIR397a/b*, *MIR857a*, *MIR389a/b*, and *MIR408* precursors (Fig. 10A); *FIT* expression was upregulated under Fe but not Cu deficiency (Fig. 10A). By contrast, all tested genes were highly upregulated when Fe and Cu deficiencies were applied simultaneously (Fig. 10A). This result suggested that simultaneous Fe and Cu deficiencies act in parallel/autonomously on the expression of Cu- and Fe-responsive genes in the root.

Cu feeding via the phloem in the shoot downregulated the expression of not only Cu *MIRNA* precursors and *CITF1* but also *FIT* in the root of plants grown under simultaneous Cu and Fe deficiencies (Fig. 10B). Feeding with Fe also downregulated not only *FIT1* expression but also that of *CITF1*; out of the Cu *MIRNA* precursors measured, the expression of all, but not the *MIR857a* precursor, was downregulated in roots of the wild-type grown under simultaneous Cu and Fe deficiencies (Fig. 10C). Together, these data suggest that Cu and Fe in the phloem can, in part, mimic each other's function in long-distance signaling.

Cu and Fe deficiencies applied simultaneously increase root Fe uptake and its delivery to shoots while high Fe reduces Cu uptake

Because Cu deficiency stimulates Fe uptake, we hypothesized that Cu deficiency in the *opt3* mutant and its lower Cu and Fe accumulation in the phloem compared to the wild-type may contribute to increased Fe accumulation in its roots and leaves. To test this hypothesis, we exposed wild-type to Cu and Fe deficiencies individually and concurrently. We then analyzed Fe accumulation in the roots and leaves of wild-type plants. We found that Cu deficiency increases Fe accumulation in both roots and leaves of wild-type Arabidopsis compared to control conditions (Fig. 11A). This finding was consistent with past observations using different

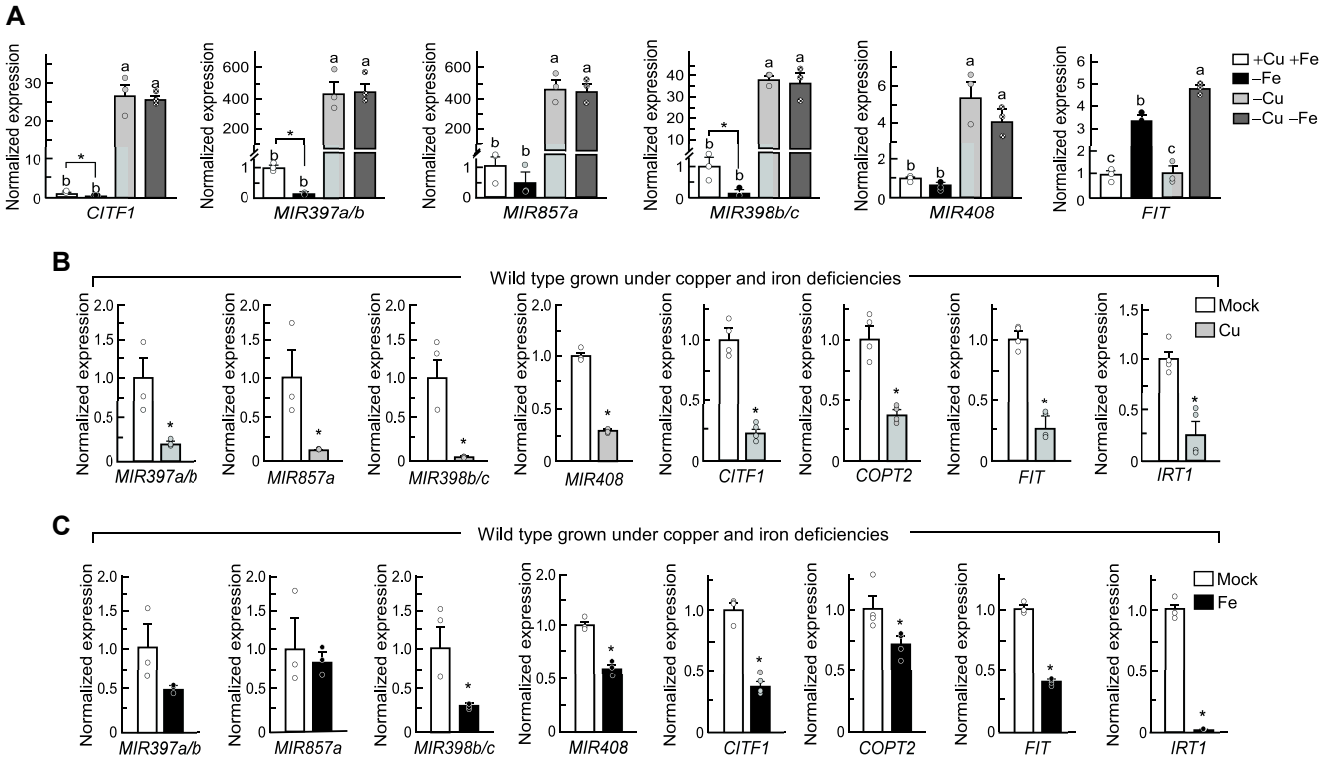

Figure 10. Cu and Fe deficiencies applied simultaneously increase the expression of *CITF1*, Cu *MIRNA*s and *FIT*. **A)** Transcript abundance of *CITF1*, the indicated Cu *MIRNA* precursors and *FIT* was analyzed in the roots of plants grown under control conditions (+ Cu) or without cooper but with Fe (−Cu) for 4 wk before tissue collection. To achieve Fe deficiency, plants were grown under control conditions for 3 wk, transferred to a solution without Fe and grown for one additional week (−Fe). For the simultaneous Fe- and Cu-deficiency treatment, plants were grown without Cu but with Fe for 3 wk and then transferred to fresh hydroponic medium lacking both Cu and Fe. Tissues were collected and analyzed after an additional week of growth (−Cu −Fe). **B)** Transcript abundance of the indicated genes in roots of wild-type grown under simultaneous Cu and Fe deficiencies after phloem feeding with Cu (gray bars) or control feeding (mock, open bars). **C)** Transcript abundance of the indicated genes in roots of the wild-type grown under simultaneous Cu and Fe deficiencies after phloem feeding with Fe (black bars) or control feeding (mock, open bars). The mock treatment for Cu feeding was MiliQ water, and the mock treatment for Fe feeding was citrate. In **A-C)**, values are means ± SE. Different lowercase letters indicate significant differences in **A)** (ANOVA followed by Tukey's HSD, JMP Pro 14 software package); asterisks in **B)** and **C)** indicate statistically significant differences from the expression of genes in mock-fed plants ($P < 0.05$, Student's *t*-test). In A-C, $n = 3$ to 4 independent experiments (PCR runs, representing an independent experimental setup where roots were pooled from three plants per experiment for RNA extraction). Data were normalized to the expression of *ACTIN2*; the expression of genes in wild-type grown under control conditions **A)** or mock-treated wild-type (**B**, C) was set to one.

experimental setups (Bernal et al. 2012; Waters et al. 2012; Kastoori Ramamurthy et al. 2018; Sheng et al. 2021). We observed a decrease in Fe accumulation in both roots and shoots under Fe deficiency. Interestingly, the simultaneous application of Cu and Fe deficiencies increased Fe accumulation in both roots and shoots compared to sole Fe-deficiency conditions (Fig. 11A). We note that plants were subjected to Fe deficiency for 1 wk, prior to which they were grown under Fe-replete conditions. Thus, it is possible that internal apoplastic Fe reserves were taken up and accounted for Fe accumulation in shoots under simultaneous Fe and Cu deficiencies. It is also possible that the simultaneous application of both Cu and Fe deficiencies stimulate an as yet unidentified high-affinity Fe uptake pathway that contributes to the root uptake of residual Fe in the medium.

Here, we also asked whether the increased accumulation of Fe in *opt3* mutant roots contributed to their lower Cu accumulation (Fig. 2A). To mimic high Fe conditions, we grew wild-type plants under control (10 μM) or high (50 μM) Fe in the medium and evaluated the accumulation of Cu. Indeed, due to the toxic nature of Fe, high Fe in the medium limited root growth while increasing root Fe levels in the wild-type compared to controls (Supplemental Figure S10, A and B). Furthermore, increased Fe concentration in the root was accompanied by a significantly lower Cu concentration in roots and shoots (Fig. 11B). While the mechanism of the effect of high Fe concentration (provided as Fe-HBED) on Cu uptake is unknown, it is possible that Fe either represses the Cu uptake system or decreases Cu availability in the outside medium. Notably, decreased Cu uptake in high Fe

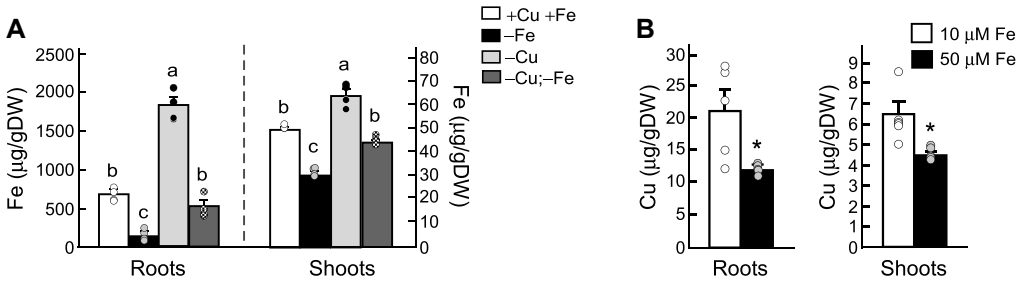

Figure 11. Cu and Fe availability in the medium influences each other's uptake and accumulation in Arabidopsis roots and shoots. **A)** Fe concentration in roots and shoots of Arabidopsis plants grown for 5 wk in control conditions (+Cu + Fe) or Cu deficiency (−Cu). To impose Fe deficiency (−Fe), a subset of plants grown in control conditions for 4 wk was transferred to the same medium without Fe and grown for one more week. For simultaneous Cu and Fe deficiencies (−Cu − Fe), plants were grown without Cu for 4 wk and then transferred to fresh hydroponic medium lacking both Cu and Fe and grown for one more week. Values are means ± SE. Different lowercase letters indicate significant differences (ANOVA followed by Tukey's HSD, JMP Pro 14 software package, $n = 3$ to 5 independent ICP-MS measurements, each representing an independent experimental setup; roots and shoots were pooled from four plants per each experimental setup to obtain one measurement). **B)** Cu concentration in roots and shoots of Arabidopsis, grown for 5 wk in control conditions (10 µM Fe) or with high Fe (50 µM Fe). Values are means ± SE from $n = 5$ ICP-MS measurements. For each measurement, tissues were pooled from four plants grown in the same container. In total, five containers from two batches of independently grown plants per condition were analyzed. Asterisks indicate statistically significant differences ($P < 0.05$, Student's *t*-test).

conditions was also documented in animal species (Klevay 2001; Ha et al. 2016).

We recognize that these experiments do not perfectly match the scenario in the *opt3* mutant that experiences internal Cu and Fe deficiencies under control conditions. Nevertheless, our results favor the intriguing suggestion that in addition to lower Fe and Cu accumulation in the phloem of the *opt3* mutant, decreased Cu accumulation in its roots and leaves contribute to its Fe overaccumulation. We also propose that high Fe in the roots of the *opt3* mutant negatively affects Cu accumulation in the roots of the mutant compared to the wild-type.

Discussion

Fe and Cu are essential micronutrients, yet they are toxic for the growth and development of all organisms if their accumulation is not highly regulated. The homeostasis of these elements is intricately related. The hallmark of this relationship in plants is the increased accumulation of Cu in plant tissues under Fe deficiency and the overaccumulation of Fe under Cu deficiency (Fig. 11 and (Bernal et al. 2012; Waters and Armbrust 2013; Kastoori Ramamurthy et al. 2018; Rai et al. 2021; Sheng et al. 2021)). The toxicity of both metals is avoided by the ability of plants to regulate Cu and Fe transport systems in response to fluctuations in Cu and Fe availability in the immediate root environment and the demands of the developing shoot. The Arabidopsis phloem companion cells-specific Fe transporter, OPT3, is involved in signaling Fe demand from shoots to roots and in transporting Fe to developing tissues such as the seed. The systemic control of Cu uptake into roots and its relationship to the systemic control of Fe uptake in plants has not yet been documented. Data presented in this article suggest the existence of systemic signaling of Cu status, its interaction with systemic Fe signaling, and the central role of OPT3 in these regulatory pathways (Fig. 12).

OPT3 transports Cu and the Cu–NA complex, but free Cu^{2+} ions are preferred substrates in heterologous systems

The nature of the transport substrate of OPT3 has been under scrutiny and is a matter of debate in the literature. OPT3 belongs to the OPT family that is phylogenetically divided into two groups: the YSL and OPT clades (Lubkowitz 2011). Analyses of the transport capabilities of some members of the Arabidopsis and rice (*Oryza sativa*) OPT family have revealed their capacity to transport synthetic tetra- and pentapeptides in heterologous systems (Osawa et al. 2006), while members of the YSL clade are expected to transport metal–chelate complexes (Osawa et al. 2006). Given the role of OPT3 in Fe homeostasis and signaling, it thought to transport either peptides that can serve as metal ligands (glutathione [GSH]) or metal-ligand complexes (metal-nicotianamine [metal-NA]) (Stacey et al. 2008; Lubkowitz 2011). Thus, our past finding that OPT3 transported free ions, Fe and Cd when expressed in *Xenopus* oocytes or the yeast Fe uptake mutant *fet3 fet4* was unexpected (Zhai et al. 2014). Consistent with the proton-coupled nature of OPT-mediated transport, our past studies and studies of our colleagues had shown that the acidification of the uptake medium stimulated OPT3-mediated inward currents (Osawa et al. 2006; Zhai et al. 2014). A construct encoding OPT3-GFP was previously heterologously expressed in yeast and mislocalized to internal vesicles rather than residing at the plasma membrane (Mendoza-Cózatl et al. 2014). To prevent OPT3-GFP processing/folding challenges and its retention at the endoplasmic reticulum, which may occur when integral plasma membrane proteins are forced to accumulate to high levels, and to avoid the use of a relatively large epitope tag (GFP) (Emmerstorfer et al. 2014), we used untagged OPT3 for functional complementation assays in yeast, reported in Zhai et al. (2014), and this article.

Here, we showed that OPT3, in addition to Fe and Cd ions (Zhai et al. 2014), also transported Cu ions when its cDNA

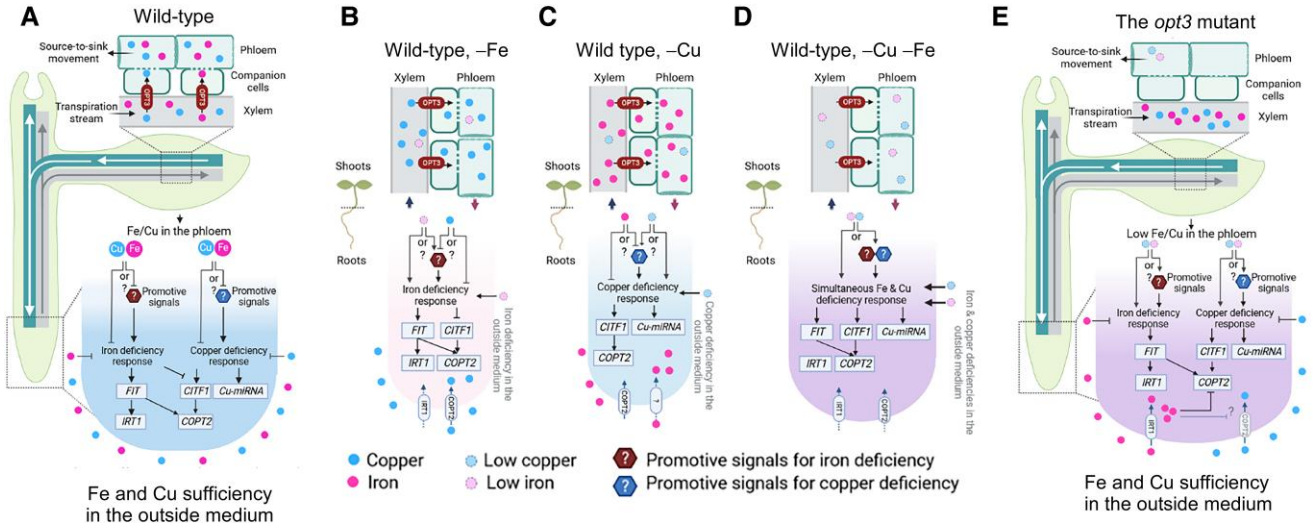

Figure 12. OPT3-facilitated Cu and Fe transport to the phloem companion cells mediates Fe–Cu crosstalk in shoot-to-root signaling. **A)** OPT3 mediates Fe and Cu loading to phloem companion cells for the distribution to sink organs, including roots. Phloem-mobile Fe and/or Cu represses the expression of Fe and Cu uptake systems, either acting directly as a repressor(s) or indirectly by sequestering or inhibiting the synthesis of a promotive signal in the phloem companion cells. **B)** Fe deficiency in the outside medium stimulates Cu accumulation in roots and leaves (Waters et al. 2012, 2014; Waters and Armbrust 2013) and Figure 11A. Under these circumstances, OPT3 loads mainly Cu to the phloem in the shoot. The concentration of Fe in the phloem decreases, which causes the upregulation of the expression of the Fe uptake system in the root. Cu availability in the phloem, provided by OPT3, fine-tunes the expression of Fe transport genes to avoid Fe overload observed in the *opt3* mutant. The repressive role of Cu on the expression of Cu and Fe uptake system can occur directly or indirectly via scavenging or inhibiting the production of a promotive signal in the phloem companion cells. A similar scenario occurs under Cu deficiency, where OPT3 mainly loads Fe to fine-tune the expression of Cu uptake genes **C)**. Simultaneous Fe and Cu deficiencies in the outside medium autonomously upregulate the expression of both Cu and Fe uptake genes as both elements are less available in phloem sap **D)**. The scenario is different in the *opt3* mutant **E)**: a lthough both Fe and Cu are available in the outside medium, the *opt3* mutant experiences simultaneous Fe and Cu deficiencies in the phloem. Low Fe accumulation in the phloem stimulates transcriptional Fe deficiency response in the root, overriding local Fe sufficiency (Fe sufficiency in the medium and high Fe accumulation in the root) that should have repressed the upregulation of Fe uptake system in the root of the *opt3* mutant. Since Fe is available in the outside medium, Fe accumulates in roots of the *opt3* mutant. Cu deficiency in the phloem, roots and leaves also leads to Fe accumulation and transcriptional Cu deficiency response. Increased Fe accumulation from both pathways, in turn, decreases Cu uptake, as shown in Figure 11B and documented in animal species (Klevay 2001; Ha et al. 2016), further altering Fe–Cu crosstalk. Figure 12 was created in Biorender.com.

was expressed in *Xenopus* oocytes or a yeast Cu transport mutant (Fig. 3). We also found that OPT3 could transport both free Cu^{2+} ions and Cu provided as Cu–NA complex (Fig. 3A). Notably, *OPT3*-expressing oocytes accumulated 4.2 times more Cu when it was provided as a free ion rather than complexed with NA, suggesting that free Cu ions are the preferred OPT3 substrate in this heterologous system. Transport capabilities and substrate preferences of OPT3 must be further tested in planta.

Our recent report showed that the members of the YSL clade of the OPT transporter family YSL3 in purple false brome (*Brachypodium distachyon*) and YS1 in maize (*Zea mays*) also transport Cu ions in *Xenopus* oocytes (Sheng et al. 2021). Unlike AtOPT3, Cu uptake by BdYSL3 was not detected when the Cu-NA complex was provided as a substrate (Sheng et al. 2021). Similar to AtOPT3, ZmYS1 was capable of transporting Cu provided as free ions as well as the Cu-NA complex; similar to AtOPT3, Cu ions were the preferred transport substrates of ZmYS1 in the *Xenopus* oocyte heterologous system (Sheng et al. 2021). Vascular tissue-localized NA efflux transporters, NAET1 and NAET2, have been identified recently in Arabidopsis (Chao et al. 2021). These transporters localize to synaptic-like vesicles in the vasculature and control Fe and Cu delivery to seeds. Therefore, as suggested by Chao et al. (2021), OPT3 and NAET1/NAET2 may act in concert in Cu/Fe and NA delivery, respectively, to the phloem. In the phloem, Cu and Fe would then form a complex with NA to facilitate mineral delivery to sink tissues. A similar scenario occurs with Fe and citrate transport to the xylem via IREG1/FPN1 and FRD3 (FERRIC REDUCTASE DEFECTIVE 3) transporters, respectively (Rogers and Guerinot 2002; Green and Rogers 2004; Morrissey et al. 2009). In the xylem, tri-Fe(III), the tri-citrate complex is formed to facilitate Fe delivery to shoots (Rellán-Álvarez et al., 2009).

Recent in silico analysis using protein secondary and tertiary structure simulations and binding affinity results of docking analyses suggested that AtOPT3 and its counterpart from maize, ZmOPT3, may transport Fe complexed with GSH (Kurt 2021). Despite this prediction, AtOPT3 does not appear to transport GSH when expressed in the yeast GSH transport mutant *hgt1*Δ, and the addition of GSH to the

Xenopus oocytes bathing medium decreases Cd transport (Zhai et al. 2014). Our finding that AtOPT3 does not transport GSH in yeast has been recently validated (Zhang et al. 2016). The AtOPT3 counterpart in rice, OsOPT7, is essential for Fe homeostasis and sources-to-sink partitioning but does not transport Fe–NA, Fe–DMA complexes, or GSH in oocytes either (Bashir et al. 2015). It is noteworthy that, unlike AtOPT3, other OPT family members in Arabidopsis, AtOPT4 and AtOPT6, as well as the closest AtOPT3 homolog from brown mustard (*Brassica juncae*), BjGt1, all transport GSH (Bogs et al. 2003; Cagnac et al. 2004; Zhang et al. 2016). Recent analyses of the Arabidopsis *opt6* mutant implicated AtOPT6 in GSH long-distance transport and delivery to sink organs, especially flowers (Wongkaew et al. 2018). It is worth noting that similar to the *opt3* mutant, the loss of AtOPT6 function delays the transition from the vegetative to the reproductive stage (Wongkaew et al. 2018). It would be interesting to test whether mineral nutrient homeostasis is disrupted in the *opt6* mutant.

Cu loading to the phloem companion cells and delivery to sinks depend on AtOPT3

The role of AtOPT3 in Fe and Cu loading to the phloem companion cells for subsequent partitioning from source to sink tissues is evidenced by the decreased accumulation of these metals in the phloem of the *opt3* mutant (Fig. 1F, G, K and Supplemental Fig. S1E) (Zhai et al. 2014). We cannot exclude the possibility that the lower phloem Cu levels in the *opt3* mutant might be a secondary consequence of a major disruption in Fe homeostasis, including strong Fe overaccumulation in source leaves. However, our finding that mature leaves of the *opt3* mutant contain higher levels of Cu while young leaves contain lower levels of Cu than the wild-type is consistent with a contribution of OPT3 to the phloem-based delivery of Cu, in addition to Fe from sources to sinks (Fig. 2A, Supplemental Fig. S3 and (Zhai et al. 2014), respectively). Here we also showed that AtOPT3 was important for Cu and Fe delivery to developing seeds and, in addition to leaves, silique valves might act as sources of these minerals for developing seeds (Fig. 2, B and C, and Supplemental Fig. S4A). This suggestion is based on our findings that silique valves of the mutant overaccumulated Fe and Cu while developing seeds accumulated less Fe (which is only detectable in the embryos vasculature) and Cu (detectable in the seed coat) compared to the wild-type (Fig. 2, B and C and Supplemental Fig. S4A). We note that, unlike Cu and Fe, Mn and Zn overaccumulated in the vasculature and both silique valves and embryos; at the same time, Zn also overaccumulated in seeds of the *opt3* mutant compared to corresponding tissues in wild-type (Figs. 1, H, I and 2B). Together, these data suggest that AtOPT3 functions in Cu and Fe but not Mn or Zn loading to the phloem and the phloem-based delivery to sink tissues.

We note that while the role of AtOPT3 and OsOPT7 in Fe delivery to seeds is evidenced by the lower Fe concentration in mature seeds (Supplemental Figure S4, B and C and (Stacey et al. 2008; Mendoza-Cózatl et al. 2014; Zhai et al. 2014; Bashir et al. 2015), Cu accumulation in mature seeds was not affected in the *opt3* mutant in our assays using ICP-MS analysis (Supplemental Fig. S4C and (Stacey et al. 2008)). However, we noted a subtle difference in Cu distribution in mature seed of the *opt3* mutant compared to wild-type using synchrotron-based X-ray F-CMT. Specifically, less Cu was associated with the vasculature of the *opt3* mutant than in wild-type, and somewhat more Cu was associated with the seed coat of the mutant (Supplemental Fig. S4B). However, this subtle difference in Cu distribution was not sufficient to account for total seed concentration.

AtOPT3 mediates Cu homeostasis and long-distance Cu transport that influence root responses to Cu deficiency

Our finding that both *opt3-2* and *opt3-3* mutant alleles accumulated less Cu in roots, young leaves compared to the wild-type (Fig. 2A and Supplemental Fig. S3) suggested that the mutant might be more sensitive to Cu deficiency and/or manifest molecular symptoms of Cu deficiency. Indeed, the size of rosette leaves of both *opt3-2* and *opt3-3* mutants, grown under Cu deficiency, was significantly smaller compared to control conditions, and their leaves were extensively chlorotic compared to the wild-type also grown without added Cu (Fig. 4F and Supplemental Fig. S6). Furthermore, consistent with our recent findings of the role of Cu in the transition to flowering (Rahmati Ishka and Vatamaniuk 2020), the *opt3* mutant failed to flower within the time frame of the experiment and developed more rosette leaves than the wild-type when grown in medium without or even with Cu (Fig. 4, C and D). Cu deficiency-associated phenotypes were rescued by transferring the mutant to medium with higher Cu concentrations (Fig. 4C to E and Supplemental Fig. S7).

We also found that the *opt3* mutant mounted molecular Cu-deficiency responses even when it was grown under control conditions. This conclusion was evidenced by the increased cupric reductase activity in roots and the upregulated expression of the Cu-deficiency regulon in roots and young leaves of the *opt3* mutant relative to wild-type (Fig. 5, Supplemental Figure S6E and Supplemental Data Sets S2 to S4). Changes in the transcriptome of mature leaves of the *opt3* mutant were indicative of neither deficiency nor sufficiency. The transcriptional Cu deficiency responses of young leaves and an unspecific response of mature leaves in the *opt3* mutant are consistent with their respective Cu concentrations (Fig. 2A, Supplemental Fig. S3 and Supplemental Data Sets S2 to S4). By contrast, Cu accumulation in the roots of the *opt3* mutant, although lower than in the wild-type, was still at the level of sufficiency (Fig. 2A and (Broadley et al. 2012)); nevertheless, *opt3* mutant toots mounted a transcriptional Cu deficiency response. Thus, we tested in which tissue, the shoot or the root, OPT3

function was required for regulating Cu-deficiency genes in the root. Using reciprocal grafting of wild-type with the *opt3* mutant, we showed that OPT3 function in the shoot regulated not only Fe but also Cu deficiency responses in the root (Fig. 8). Furthermore, we showed that Cu feeding via the phloem in the shoot downregulated the expression of the Cu deficiency markers, *CITF1*, *COPT2* and Cu *MIRNA* precursors in the root of the *opt3* mutant that constitutively overexpresses Cu deficiency marker genes even when grown under control conditions. Cu feeding via the phloem in the shoot also downregulated the expression of *CITF1*, *COPT2*, and Cu *MIRNA* precursors in the root of the Cu-deficient wild-type. Together, these results suggested that Cu availability in the phloem in the shoot is important for regulating Cu-deficiency responsive genes in the root.

When interpreting these results, we considered two nonmutually exclusive scenarios: (i) the nutritional effect of phloem Cu and (ii) the signaling role of phloem Cu. External Cu rescued the Cu-deficiency phenotypes of the *opt3* mutant (Figs. 4, C to E, 7 and Supplemental Fig. S7). A trivial explanation is that Cu was lacking (in at least some cells) and can be provided. Likewise, the direct phloem feeding of Cu might be causing Cu transport from the shoots to the roots, where it alleviates Cu deficiency, which in turn suppresses the expression of Cu deficiency-induced genes in the roots of the *opt3* mutant (Fig. 9D). However, grafting results are more difficult to interpret as a nutritional effect of Cu. Grafting *opt3* shoots onto wild-type rootstocks caused elevated expression of Cu deficiency-regulated genes in roots (Fig. 8). It is difficult to explain this as a nutritional effect, since the wild-type roots experienced Cu sufficiency during the entire experiment, and thus, a systemic signaling role for Cu is plausible.

Furthermore, as discussed in detail below, we showed that feeding Cu via the phloem in the shoot of the *opt3* mutant suppressed the expression of Fe deficiency marker genes in the roots, even though *opt3* mutant roots overaccumulate Fe, and plants were grown in control conditions (Fig. 9D). This finding is also consistent with the systemic signaling role of Cu and its crosstalk with systemic Fe signaling.

The gene encoding the upstream regulator of *CITF1*, *COPT2*, and Cu *MIRNA* precursors, *SPL7*, is expressed in the vascular tissues of both shoot and roots, locally senses Cu availability, and transmits it to surrounding cells (Araki et al. 2018). In the root, *SPL7* is detected in the pericycle (Long et al. 2010). Considering that the phloem pole pericycle plays a major role in regulating symplastic phloem unloading in the root (Ross-Elliott et al. 2017), it is possible that SPL7 senses the availability of phloem-arrived Cu in the pericycle to regulate the expression of *CITF1*, *COPT2*, Cu *MIRNA* precursors, as well as other SPL7 targets in the root.

It is noteworthy that FIT cooperates with bHLH38, bHLH39, bHLH100 and bHLH101 to control the upregulation of Cu uptake genes (*COPT2*, *FRO4* and *FRO5*) under Fe deficiency (Cai et al. 2021). All the above-cited genes were also upregulated in the roots of the *opt3* mutant (Fig. 5B and Supplemental Data Set S2). Therefore, it is possible that some of the Cu-deficiency responses (e.g. *COPT2*, *FRO4*, and *FRO5*) of the *opt3* mutant roots are regulated by FIT, bHLH38, bHLH39, bHLH100, and bHLH101 as well.

Cu and Fe levels in the phloem companion cells and Fe–Cu crosstalk in shoot-to-root signaling depends on AtOPT3

In addition to AtOPT3 mediating Cu transport and contributing to Cu accumulation in the phloem, AtOPT3 function was also important not only for feeding the developing sinks with Cu but also for conveying the Cu status of the shoot to the root. In addition, one of the unexpected outcomes of our study was finding that feeding with Cu via the phloem in the shoot downregulated the expression of both Cu- and Fe-deficiency markers in *opt3* mutant roots (Fig. 9D). Likewise, Fe feeding via the phloem in the shoot downregulated the expression of *FIT* and *IRT1* as well as *CITF1* and *COPT2* in *opt3* mutant roots (Fig. 9C).

We note that the *opt3* mutant has a lower concentration of both Cu and Fe in the phloem and, thus, provides a sensitized genetic background for phloem-feeding experiments with Cu or Fe. Therefore, we used wild-type plants, subjected them to Cu and Fe deficiencies individually or simultaneously, and fed them with either Cu or Fe via the phloem in the shoot. We found that either Cu or Fe phloem feeding regulated the expression of both Cu and Fe deficiency-responsive genes in roots of Fe or Cu-deficient plants in the expected manner (Figs. 9, A and B and 10, B and C). Specifically, the expression of tested genes typically upregulated by Cu deficiency (*COPT2*, *CITF1*, and Cu *MIRNA* precursors) or by Fe deficiency (*IRT1*, *FIT*), was downregulated in roots by feeding with Cu or Fe. The expression of *CITF1*, which is downregulated in plant roots by Fe deficiency, was upregulated in roots of Fe-fed, Fe-deficient plants (Fig. 9A). Interestingly, even though Cu deficiency does not seem to affect the expression of *FIT* and *IRT1* in wild-type Arabidopsis (Bernal et al. 2012) and Fig. 10A for *FIT* expression, Cu feeding via the phloem in the shoot downregulated the expression of these genes in roots of Cu-deficient plants (Fig. 9B). Considering that Cu deficiency increases Fe concentration in the roots of Arabidopsis via unknown transport system(s) (Fig. 11A and (Waters et al. 2012, 2014; Waters and Armbrust 2013)), it is tempting to speculate that the FIT-IRT1 module contributes to this system; hence, the decreased expression of *FIT* and *IRT1* in roots of Cu-fed, Cu-deficient plants would be needed to stabilize (fine-tune) Fe uptake to avoid Fe toxicity (further detailed below and discussed in Fig. 12). Together, these findings raise an intriguing possibility that Fe and Cu in the phloem can, in part, substitute for each other's signaling function in regulating the expression of Cu and Fe uptake genes in the root to fine-tune these minerals uptake in response to plant needs (Fig. 12).

We do not propose that Cu and Fe act interchangeably in the phloem, as wild-type plants that are Cu-deficient (and not Fe-deficient) induce Cu deficiency responses in roots

and vice versa. Our finding that Fe deficiency significantly increased the expression of the already highly expressed Fe uptake system in *opt3* mutant roots (Fig. 5D) is especially relevant for understanding the proposed model of AtOPT3-mediated Cu–Fe crosstalk in long-distance signaling, as discussed below (Fig. 12).

We propose that in wild-type Arabidopsis grown under combined Cu and Fe sufficiency, Cu and Fe ions, taken up by the root and delivered to the shoot, are loaded into phloem companion cells in leaves by AtOPT3 to convey Cu/Fe sufficiency to the root (Fig. 12A). Under Fe-deficiency conditions, Fe is limited, while the concentration of Cu in roots and leaves increases due to the increased Cu absorption by roots under Fe deficiency (Fig. 12B) and (Waters et al. 2012,2014; Waters and Armbrust 2013). Under these circumstances, AtOPT3 loads mainly Cu into phloem companion cells. Phloem Cu (or Cu-related/derived signal, or lack thereof) decreases the expression of the Fe deficiency uptake system to avoid Fe overload, such as in *opt3* mutants, fine-tuning Fe uptake to the needs of the plant. Consistent with this suggestion is our finding that the expression of *FIT* and *IRT1* was significantly higher in the *opt3* mutant compared to the wild-type under Fe deficiency (Fig. 5D).

Similarly, under Cu deficiency, AtOPT3 loads mainly Fe into phloem companion cells, since Cu is limited (Fig. 12C). This AtOPT3 function fine-tunes the expression of Fe and Cu transport systems to ensure adequate Fe/Cu uptake while preventing toxicity. It is noteworthy that unlike Cu or Fe feeding via the vasculature in the shoot, the function of AtOPT3 in the wild-type does not entirely suppress Cu or Fe uptake systems in the root under reciprocal deficiency, since Cu or Fe uptake systems are still upregulated (Fig. 12, B and C). It is possible that the concentration of Fe or Cu in the phloem in Arabidopsis grown under Cu or Fe deficiency may not be sufficient to fully repress the expression of Cu or Fe uptake genes in the root. It is also possible that the sink strength and competition (roots or shoot apices and developing leaves) are also important contributing factors that determine the amount of Cu and Fe (as well as other components of the phloem sap) recirculated to roots via the phloem to influence Fe or Cu uptake under reciprocal deficiency.

Concerning the *opt3* mutant, we propose that the constitutive expression of Cu and Fe uptake systems in its roots originates from constitutive Cu and Fe deficiencies in the leaf phloem, most likely the phloem companion cells (Fig. 12, D and E). Cu and Fe deficiencies, co-occurring in the phloem of the *opt3* mutant, act autonomously in regulating Cu- and Fe-deficiency genes in the roots. This suggestion is based on our finding that the expression of *CITF1* and Cu *MIRNA* precursors, which are normally downregulated by Fe deficiency while upregulated by Cu deficiency when applied independently, was upregulated under simultaneous imposition of both deficiencies (Figs. 10A and 12D). Likewise, although *FIT* was upregulated by Fe deficiency and did not respond transcriptionally to Cu deficiency, it was upregulated by the simultaneous application of Cu and Fe deficiencies (Figs. 10A and 12D).

A question remains about how Cu and Fe act in systemic signaling. Cu/Fe availability in the phloem may be communicated via a common transduction pathway and/or metal-binding ligand. The putative Fe sensors HRZs (Haemerythrin motif-containing Really Interesting New Gene (RING)- and Zinc-finger proteins)/BTS (BRUTUS) and IDEF1 (IDE-BINDING FACTOR 1) in Arabidopsis and rice bind not only ionic Fe^{2+} but also other transition metals and act in the root to regulate the Fe uptake system (Selote et al. 2014; Kobayashi 2019). Phloem sap contains potential Fe- and Cu-binding ligands such as NA and GSH (reviewed in Gayomba et al. (2015)). Notably, the *nas4x* mutant of Arabidopsis, lacking four NA synthase genes, overaccumulates Fe in the vasculature, similar to the *opt3* mutant (Nguyen et al. 2022). Unlike the *opt3* mutant, Cu accumulation in the vasculature of the *nas4x* mutant was not observed, suggesting that in Arabidopsis, NA contributes mainly to Fe homeostasis (Klatte et al. 2009; Nguyen et al. 2022). While roots of the *nas4x* mutant exhibit somewhat elevated levels of *FIT*, *IRT1*, and *FRO2* expression compared to wild-type both grown under control conditions, unlike the *opt3* mutant (Fig. 5D), the expression of Fe uptake genes in *nas4x* roots does not increase further under Fe deficiency (Klatte et al. 2009). It is tempting to speculate that Cu loaded by OPT3 to the phloem in the *nas4x* mutant controls the expression of Fe uptake genes in its roots. The *nas4x* mutant will provide an excellent complementary system for studying the crosstalk between Cu and Fe in systemic signaling. A new family of phloem mobile peptides, IMA/FEP, was proposed to coordinate systemic Fe deficiency signaling. Their contribution to the crosstalk between Fe and Cu systemic signaling is unknown (Grillet et al. 2018; Hirayama et al. 2018).

While our data are consistent with the repressive role of phloem-associated Fe and Cu in systemic signaling and the expression of Fe and Cu uptake systems in the root, a promotive mechanism of systemic signaling has been brought forward as well (Grusak and Pezeshgi 1996; Vert et al. 2003; Kumar et al. 2017). In this mechanism, Fe-sufficient status in the shoot would prevent a release of the promotive systemic signal, and Fe deficiency-responsive genes will not be expressed in the root. Considering this scenario, it is possible that Fe and/or Cu in the phloem companion cells would sequester or inhibit the biosynthesis of the promotive signal(s), preventing the upregulation of genes encoding the root Fe and/or Cu uptake systems (Fig. 12). We note that both repressive and promotive mechanisms rely on the availability of Fe and Cu in the phloem, most likely in phloem companion cells.

To conclude, our studies assigned new functions to AtOPT3 in contributing to Cu loading into the phloem, subsequent distribution to sink tissues and systemic signaling of Cu deficiency. We also discovered that Cu can partially substitute for Fe in long-distance signaling. We also showed the important role of OPT3 in Cu-Fe crosstalk in normal homeostasis of both elements. Understanding the basic

mechanisms plants use to coordinate Fe and Cu demands with their uptake, transport and utilization will provide promising avenues for targeted biofortification strategies directed at increasing Fe contents in the edible portions of crops and improving agricultural productivity on Fe- and Cu-deficient soils.

Materials and methods

Plant material and growth conditions

Arabidopsis (*Arabidopsis thaliana*) accession Columbia 0 (Col-0) and a previously described *opt3*-3T-DNA insertion mutant in Col-0 (SALK_058794C; (Zhai et al. 2014)) were obtained from ABRC. A previously described *opt3-2* T-DNA allele (SALK_021168, (Stacey et al. 2008)) in Col-0 is a generous gift from the David Mendoza-Cozatl lab (University of Missouri) and was used in Supplemental Figures S3 and S6A. For soil-grown plants, seeds were directly sown onto Lambert 111 all-purpose peat moss (lambertpeatmoss.com/en, product code 64980 2512) and irrigated with regular NPK fertilizer. For Cu-deficiency treatments, plants were either grown on half-strength Murashige and Skoog (MS) medium (Sigma-Aldrich, M5519) with 1% (w/v) sucrose and 0.7% (w/v) agar or hydroponically in a medium containing 1.25 mM KNO_3, 0.625 mM $KH2PO_4$, 0.5 mM $MgSO_4$, 0.5 mM $Ca(NO_3)$ and the following micronutrients: 17.5 µM H_3BO_3, 3.5 µM $MnCl_2$, 0.25 µM $ZnSO_4$, 0.05 µM $NaMoO_4$, 2.5 µM NaCl, and 0.0025 µM $CoCl_2$ (Arteca and Arteca 2000), and the indicated concentrations of $CuSO_4$ with 125 nM Cu considered as control. Fe (10 µM) was provided as Fe(III) HBED (N, N′-Di (2-hydroxybenzyl) ethylenediamine-N, N′-diacetic acid). The pH of the hydroponic medium was adjusted to 5.6 with 1 M KOH (Yan et al. 2017). For growing plants hydroponically, seeds were surface sterilized as described in Jung et al. (2011) before sowing onto 0.7% (w/v) agar aliquoted in 10-µL pipette tips. Pipette tips were cut before placing them into floats made of foam boards. Seedling roots were immersed into the hydroponic solution after 7 to 8 d of growth. To ensure that both the wild-type and the *opt3-3* mutant were treated at the same growth stage, all seedlings or plants were transferred when the rosette reached 50% of the final size (principal growth stage 3.5 as documented in Boyes et al. (2001)). In this case, the wild-type and the *opt3-3* plants were transferred 3 and 4 wk after sowing seeds, respectively. The solution was replaced weekly and was replaced one more time 24 h before collecting samples. All plants were grown in a growth chamber at 22 °C and 75% humidity, under a 14-h light/10-h dark photoperiod at a photon flux density of 110 µmol m^{-2} s^{-1} achieved with fluorescent light bulbs Philips F32T8/TL741.

High-throughput RNA sequencing and analysis

Wild-type Arabidopsis and *opt3-3* plants were grown hydroponically with 0.125 µM $CuSO_4$ for 4 wk. Total RNA was isolated from roots, mature, and young leaves using TRIzol reagent (Invitrogen). Tissues were pooled from four plants grown in the same container for each replicate, and three containers were used per genotype. Strand-specific RNA-seq libraries were constructed using 3 µg of total RNA according to procedures described previously (Zhong et al. 2011). RNA-seq libraries were sequenced on an Illumina HiSeq 2500 system as single-end reads. Three replicates were used for RNA-seq. Trimmomatic (Bolger et al. 2014) was employed to remove adaptor and low-quality sequences from the Illumina raw reads. Reads shorter than 40 bp were discarded. The resulting clean reads were aligned to the ribosomal RNA database using Bowtie with up to 3 mismatches allowed (Langmead et al. 2009; Quast et al. 2013), and mapped reads were discarded. The final clean reads were aligned to the Arabidopsis genome sequence (TAIR 10) using TopHat with up to 1 mismatch allowed (Trapnell et al. 2009). Finally, the counts of mapped reads for each gene model from each sample were derived and normalized to RPKM (reads per kilobase of exon model per million mapped reads). DESeq2 was used to identify DEGs from the raw count data (Love et al. 2014). Raw *P*-values were corrected for multiple testing using an FDR (Benjamini and Hochberg 1995). Genes with an FDR < 0.05 and up- and downregulation cutoff of 1.5 and 0.67, respectively, were regarded as DEGs. Gene ontology (GO) term enrichment and gene functional classification analyses were performed using Plant MetGenMap (Joung et al. 2009).

ICP-MS analysis

Root and shoot tissues were collected from 5-wk-old plants grown hydroponically as described above. The seeds and siliques were collected from 11 to 12-wk-old plants grown on soil as described above. Fe and other elements were desorbed from root cell walls by washing roots in 10 mM EDTA for 5 min and with a solution with 0.3 mM bathophenanthroline disulfonate (BPS) and 5.7 mM sodium dithionite for 10 min, followed by three consecutive washes in deionized water. Fully expanded mature leaves (three leaves/plant) and two-to-three upmost leaves less than 5 mm long (young leaves) were rinsed with deionized water three times and then pooled separately as mature leaves and young leaves. Dry seeds and valves were collected from plants grown on soil, and seeds were separated from the valves with a 500-µm mesh. All samples were dried in an 80 °C oven before measuring their weight. Elemental analysis was performed using inductively coupled plasma mass spectroscopy (ICP-MS; Agilent 7500).

RT-qPCR analysis

Roots and leaves were collected from plants at Zeitgeber time 7 (ZT, ZT0 being defined as lights-on) and flash-frozen in liquid nitrogen before homogenization. Total RNA was isolated using TRIzol reagent (Invitrogen) according to the manufacturer's instructions. First-strand cDNA templates used for qPCR analysis were synthesized using an AffinityScript

QPCR cDNA synthesis kit (Agilent Technologies). One µg of total RNA was treated with DNase I (New England Biolabs) prior to first-strand cDNA synthesis to eliminate genomic DNA contamination. Real-time qPCR analysis was performed in a total volume of 15 µL containing 1× iQSYBR GreenSupermix (Bio-Rad), 500 nM of each PCR primer and 2 µL of 15× diluted cDNA templates using s CFX96 real-time PCR system (Bio-Rad) as described (Gayomba et al. 2013). Data were normalized to the expression of *ACTIN2* (At3g18780), whose expression was stable under the investigated conditions and in studied genotypes (Supplemental Data Set S5). The fold-difference ($2^{-\Delta\Delta Ct}$) and the statistical parameters were calculated using the CFX Manager Software, version 3.1 (Bio-Rad). Sequences of the primer sets used in this study are listed in Supplemental Table S1.

Grafting experiments

The grafting method was described previously with slight modifications (Marsch-Martínez et al. 2013). All procedures were performed under a Leica S6E microscope. Briefly, wild-type and *opt3-3* seeds were germinated and grown vertically on half-strength MS medium with 0.5% (w/v) sucrose for 6 to 7 d. Cotyledons were removed using sterile scalpels with No.11 blades right before grafting. The scions and rootstocks were then separated and moved to half-strength MS plates with 0.5% (w/v) sucrose and 0.7% (w/v) agar for alignment. After grafting, the plants were grown vertically on plates for another 10 d. Successfully grafted plants without adventitious roots above the graft junction were transferred to the hydroponic system with 0.25 µM $CuSO_4$ for 24 d before qPCR analysis.

Synchrotron X-ray fluorescence imaging

Fresh samples were detached immediately before analysis and placed in a wet chamber made between two layers of metal-free Kapton film and mounted onto 35-mm slide frames. The spatial distribution of Cu and Fe was imaged via SXRF microscopy at the F3 station of the Cornell High Energy Synchrotron Source (CHESS). The 2D Cu and Fe raster maps were acquired at 25-µm resolution, 0.2 s/pixel dwell time using a focused, monochromatic incident X-ray beam at 12.8 keV and photon flux of ~10^{10}photons/s. The monochromatic beam was generated with 0.6% energy bandwidth multilayers. Focusing was achieved using a single-bounce monocapillary, PEB605, fabricated at CHESS. These settings did not cause detectable damage to plant tissues within the 6 to 9-h scans required to analyze the complete set of samples. Element-specific XRF was detected using a Vortex ME-4 silicon drift detector. Quantifications were conducted by calibrating using a thin Cu foil film standard (15.9 µg Cu/cm^2, the metal was deposited on 6.3-µm thick Mylar) during each experiment and concentrations were expressed as µg cm^{-2}. Data were processed with the software Praxes, developed at CHESS and employing PyMCA libraries in batch mode (Solé et al. 2007).

Synchrotron-based confocal XRF microscopy

Confocal XRF experiments were obtained at beamline 5-ID (SRX) at National Synchrotron Light Source (NSLS-II) in Upton, NY. The beamline monochromator and focusing optics were employed to deliver 3×10^{11} photons/second in a 1×1-μm^2 beam, with an incident beam energy of 10.0 keV and bandwidth of approximately 1 eV. Confocal geometry was achieved by placing a collimating channel array (CCA) (Agyeman-Budu et al. 2016) onto a single-element Vortex SDD detector perpendicular to the beam. The sample stage was oriented such that the horizontal translation axis of the stage was 35 degrees from that of the incident beam and 55 degrees from the detector axis. The particular CCA employed for these measurements has a series of 175, 2-µm channels etched into a 1-mm thick germanium substrate, etched to an approximate depth of 300 µm. The working distance between the sample and the optic was 1.5 mm. Due to the finite width of the optic at its front tip, the maximum probe depth of the system in this configuration was 0.8 mm. Quantitative calibration of the confocal XRF system was achieved by methods described in Malzer and Kanngießer (2005) and Mantouvalou et al. (2012).

Synchrotron-based X-ray fluorescence computed microtomography

Internal distributions of Cu, Fe, and other micronutrient elements in wild-type and *opt3-3* mutant seeds were measured in vivo by synchrotron-based X-ray F-CMT at the X-ray Fluorescence Microprobe (XFM) beamline at NSLS-II. XFM (4-BM) beamline is designed for monochromatic operation in the 2.3–23 keV range and optimized for high-quality, spatially-resolved X-ray absorption spectroscopy (sulfur to technetium K-edges) in conjunction with element-specific imaging and microdiffraction. XFM beamline can also be operated in a pink beam "imaging" mode that delivers a 1-micron spot with up to 1000× more flux than the XFM monochromatic beam. XFM-filtered pink beam (12 to 20 keV broadband) was focused by Kirkpatrick-Baez (KB) mirrors to a 1-µm spot for F-CMT measurements of seeds. Seeds were mounted to a quartz post that interfaces with a Huber goniometer head on a rotation stage attached to a fast-scanning translation stage. F-CMT images were acquired at the seed center by rotating and translating the specimen in the microbeam while recording the fluorescence intensities with a Hitachi 4-element Vortex SDD coupled to Quantum Detectors Xspress3 electronics. F-CMT data were collected using 0.75 to 3.0-degree angular steps, 2 to 8-µm translation steps and 50 ms dwell time. Tomographic image reconstructions using a conventional filtered back projection algorithm were processed using a tomo-Py plugin to GSE Mapviewer in the LARCH package (Newville 2013). Thin-film standard reference materials (SRM 1832 & 1833) were measured as part of the data set to establish elemental sensitivities (counts per second per mg cm^{-2}). The intensity of elements between the wild-type and *opt3* was set to the same scale.

Cu uptake in *Xenopus laevis* oocytes

Oocyte harvesting, cRNA synthesis, microinjections, and *OPT3* expression in *Xenopus* oocytes were performed as described previously (Zhai et al. 2014). All animal procedures were performed in accordance with Cornell University IACUC Protocol number 2017-0139. *X. laevis* oocytes were injected with 50 nL of water (control) or 50 nL of water containing 50 ng of *OPT3* cRNA and incubated in ND96 solution at 18 °C for 4 d prior to uptake measurements. The basal uptake solution consisted of a modified ND96 solution containing 96 mM NaCl, 1 mM KCl, 0.9 mM $CaCl_2$, buffered with 5 mM 2-(N-morpholino) ethanesulfonic acid/NaOH to pH 6.0, as previous studies determined these conditions were suitable to minimize endogenous transport in oocytes (Zhai et al. 2014; Sheng et al. 2021). The uptake solution was supplemented with 25 µM Cu–NA or 100 µM $CuSO_4$ (the final free Cu^{2+} activity in the uptake solution being estimated to be 35 µM as determined by GEOCHEM-EZ (Shaff et al. 2010)). Each sample contained 8 to 10 oocytes, with five replicates per data point. At a given time point, the uptake was terminated by washing oocytes six consecutive times with an ice-cold basal uptake solution. Oocytes were collected and samples were digested in 100 µL 70% (w/v) $HClO_4$, resuspended in 5 mL of 0.1 M nitric acid and analyzed by ICP-MS (Sciex ICP-MS). Resting membrane potentials were measured as described previously (Zhai et al. 2014).

Functional complementation assays in *Saccharomyces cerevisiae*

Budding yeast (*S. cerevisiae*) wild-type strain SEY6210 (*MATa ura3-52 leu2-3, −112 his3Δ200 trp1Δ901 lys2-801 suc2Δ9*) and the *ctr1Δctr2Δctr3Δ* triple mutant (*MATa ura3-52 his3Δ200 trp1-901 ctr1::ura3::Knr ctr2::HIS3 ctr3::TRP1*) were used for functional complementation assays. The *YES3-Gate-OPT3* construct or *YES3-Gate* lacking the cDNA insert were transformed into the appropriate yeast strain using a Frozen-EZ Yeast Transformation II kit (Zymo Research). Transformants were selected for uracil prototrophy on YNB medium containing 6.7% (w/v) yeast nitrogen base without amino acids (Difco), 0.77% (w/v) CSM–URA, 0.5% (w/v) NaCl, 2% glucose, 2% (w/v) agar.

Functional complementation assays included analyses of the respiration competence and Cu accumulation of yeast cells as described (Jung et al. 2012). Specifically, the respiration competence of different colonies was tested by their ability to grow on non-fermentable carbon sources (Dancis et al. 1994). Accordingly, different colonies harboring the appropriate constructs were grown in liquid YNB–URA to an $OD_{600\ nm} = 1.0$, diluted 10-fold serially, and spotted onto YPEG medium containing 1% (w/v) yeast extract, 2% (w/v) bacto-peptone, 3% (v/v) glycerol, 2% (v/v) ethanol, and 2% (w/v) agar and the indicated concentrations of $CuSO_4$. Plates were incubated for 3 d at 30 °C.

Different yeast colonies were grown to exponential log phase in liquid YNB medium described above to analyze Cu accumulation. An aliquot (150 µL) of an overnight culture was inoculated into 20 mL of fresh YNB medium with 20 µM $CuSO_4$ and cells were grown at 30 °C. After 24 h, cells were collected by centrifugation at 4,000 × *g* for 10 min at 4 °C, washed with deionized water before Cu was desorbed from yeast cell wall by washings in desorbing buffer containing 1 mM EDTA and 100 µM of BCS, pH8.0. Cells were then washed twice in deionized water and collected by centrifugation. The cell pellet was dried, digested by heating with a combination of purified concentrated nitric and perchloric acids, and finally dissolved in 10 mL of 5% (v/v) nitric acid. The concentration of Cu in processed yeast cells was analyzed by ICP-MS (Agilent 7500).

Collection of phloem sap

Phloem sap was collected from wild-type and *opt3-3* mutant plants grown hydroponically at the late vegetative stage as described (Zhai et al. 2014). Briefly, leaves # 9 and 10 collected from one plant were pooled together, and xylem sap was allowed to leak out by placing the petioles in a tube filled with 300 µL of deionized water and incubated in an illuminated growth chamber for 15 min, followed by further incubation in darkness for 1 h. To collect phloem sap, the petioles were then recut in 5 mM Na_2-EDTA (pH 7.5) under low light before placing the petioles in pre-weighed Eppendorf tubes containing 250 µL of 5 mM Na_2-EDTA (pH 7.5). Leaves were then incubated in darkness for 1 h in a high-humidity chamber lined with wet paper towels and sealed with vaseline. Samples with the collected phloem sap were weighed again to determine the volume of phloem sap obtained per sample to calculate concentrations of Cu or potassium (abundant in the phloem) after ICP-MS.

Cu and Fe feeding to the phloem

The phloem-feeding procedure was performed as described (Oparka et al. 1994, 1995; Knox 2019). The procedure is based on the abrasion of a source leaf vein that results in some phloem "trapping" of the applied sample. To test the effectiveness of phloem loading, the phloem tracer carboxyfluorescein diacetate succinimidyl ester (CFDA) was used: after diffusing into plant cells, CFDA cleaved by cellular esterases into a membrane-impermeable form, CF (Grignon et al. 1989). Wild-type Arabidopsis was grown hydroponically in control conditions for 33 d. Ten microliters of 10 mM CFDA were applied to the leaf surface around the major vein of six to seven bottommost leaves before the leaf surface at the major vein was abrased with a carbon steel blade. CF-mediated fluorescence in roots was visualized after 6 h using a FITC filter set of the Axio Imager M2 microscope equipped with a motorized Z-drive (Zeiss). Images were collected using a high-resolution 25 AxioCam MR Camera and processed using Adobe Photoshop software package, version 12.0.

For Fe or Cu phloem-feeding, wild-type Arabidopsis was grown hydroponically with or without 125 nM $CuSO_4$ for 33 d. To impose Fe deficiency, plants were grown hydroponically in a control solution for 31 d and then a subset was

transferred to fresh medium without Fe and grown for an additional 2 d. The *opt3* mutant was grown hydroponically under control conditions for 33 d. Ten microliters of 5 mM $CuSO_4$ or 10 mM $FeCl_2$ dissolved in 10 mM citrate were applied to the major vein of 6 to 7 bottommost leaves before the leaf surface at the major vein was abrased with a carbon steel blade. For control, water (a mock treatment for $CuSO_4$) or 10 mM citrate (a mock treatment for Fe(II)-citrate) were fed to the phloem as described above. This procedure was performed on eight fully developed leaves per plant. In all experiments, roots were collected after 24 h of phloem-feeding and at ZT4-5. Roots were pooled from four plants per experiment and all experiments were repeated at least two times.

Protein extraction and immunoblot analysis

The procedures for total protein extraction were modified from Sivitz et al. (2011). One-hundred mg of fresh root samples was frozen in liquid nitrogen and ground with a bead mill homogenizer (Omni Bead Ruptor 12). Total proteins were then extracted from the ground tissues by adding 300 µL protein extraction buffer containing 5% (w/v) SDS, 5% (v/v) b-mercaptoethanol, 50 mM Tris–HCl (pH 7.4), 1× protease inhibitor cocktail (Sigma-Aldrich, P9599), 40 mM MG-132, (Sigma-Aldrich), and 2 mM phenylmethylsulfonyl fluoride (PMSF, Millipore-Sigma). The protein extracts were centrifuged at 4,000 × *g* at 4 °C for 15 min, and total cellular proteins were separated from cell debris. Protein concentration was measured using the Bradford assay (Bradford 1976). The samples were then boiled at 95 °C for 10 min before electrophoresis. For each sample, 5 µL total proteins were separated on a 12% SDS-PAGE and were transferred onto a nitrocellulose membrane (BIORAD) by electroblotting. The immunoblotting procedures were described previously with slight modifications (Kim et al. 2010). The membranes were first blocked in EveryBlot Blocking Buffer (BIORAD). For immunodetection of IRT1, the nitrocellulose blots were probed with primary goat polyclonal anti-IRT1 antibody (1:5,000 dilution, Agrisera AS11-1780), and then with secondary HRP-conjugated antigoat-IgG antibody (1:10,000, Rockland Immunochemicals). For the immunodetection of actin, the nitrocellulose blots were probed with a primary mouse-monoclonal anti-actin antibody (1:5,000 dilution, Sigma-Adrich) and then a secondary, HRP-conjugated goat anti-mouse IgG antibody (1:10,000 Rockland Immunochemicals). In both cases, immunoreactive bands were visualized with Clarity Max ECL blotting substrates (BIORAD).

Statistical analysis

Statistical analyses of experimental data were performed using the ANOVA single-factor analysis and Tukey HSD using JMP Pro 14 (SAS Institute Inc., Cary, NC, 1989 to 2007). Student's *t*-test was used when indicated for comparing the means between the two groups.

Accession numbers

Sequence data of the genes from this article can be found in the Arabidopsis Genome Initiative or GenBank/EMBL databases under the following accession numbers: *OPT3* (At4g16370), *CITF1* (At1g71200), *FRO4* (At5g23980), FRO5 (At5g23990), *COPT1* (At5g59030), *COPT2* (At3g46900), *YSL1* (At4g24120), *YSL2* (At5g24380), *YSL3* (At5g53550), *CSD1* (At1g08830), *CSD2* (At2g28190), *IRT1* (At4g19690), *FRO2* (At1g01580), *FRO6* (At5g49730), *FRO7* (AT5g49740), *FSD1* (At4g25100), *ARPN* (At2g02850), *BCB* (At5g20230), *CCS1* (At1g12520), *UCC2* (At2g44790), *FER1* (At5g01600), *FER3* (At3g65090), *FER4* (At2g40300), *ZIP2* (At5g59520), *bHLH23* (At4g28790), TCH4 (At5g57560), *BTSL1* (At1g74770), *ZAT12* (At5g59820), *FEP2/IMA2* (At1g47395), *FEP1/IMA3* (At2g30766), *IREG2/FPN2* (At5g03570), *VTL1* (At1g21140), *VTL2* (At1g76800), *VTL5* (At3g25190), *NAS3* (At1g09240), *PETE2* (At1g20340), *MT1B* (At5g56795), *NRT2.7* (At5g14570), *MT1B* (At5g56795), *MT1A* (At1g07600), *MT2A* (At3g09390), At2g47010, At4g10500, At1g31710, At1g32350, At5G02670, and At5g05250.

Raw RNA-Seq reads have been deposited into the NCBI BioProject database under accession PRJNA930736 (http://www.ncbi.nlm.nih.gov/bioproject/930736).

Acknowledgments

We thank Prof. Mary-Lou Guerinot (Dartmouth College, USA) for providing seed of the *fit-2* mutant and for constructive comments on the manuscript. We thank Prof. David Mendoza-Cózatl (University of Missouri) for providing seeds of the *opt3-2* mutant. We thank a former member of the Vatamaniuk lab, Nanditha Vimalakumari, for her contribution to Figure 3 and all current lab members for constructive comments on the manuscript. We thank Prof. Margaret Frank and her Ph.D. student, Hannah Thomas (Cornell University), for assisting with the phloem-feeding experiments. We thank Dr. John Grazul at the Cornell Center for Materials Research (CCMR) for assisting in the preparation of samples for 2D-CXRF. The CCMR facility is supported by the National Science Foundation under Award Number DMR-1719875. Parts of this research used the XFM and SRX Beamlines of the National Synchrotron Light Source II, a U.S. Department of Energy (DOE) Office of Science User Facility operated for the DOE Office of Science by Brookhaven National Laboratory under Contract No. DE-SC0012704. This work is based upon research conducted at the Cornell High Energy Synchrotron Source (CHESS), which during the period of this study was supported by the National Science Foundation Division of Materials Research award #-1332208; the Center for High Energy X-ray Sciences (CHEXS) is presently supported by the National Science Foundation Division of Materials Research award #1829070.

Author contributions

J.-C.C. and O.K.V. designed experiments; all authors contributed to different experiments presented in this manuscript.

J.C. and O.K.V. wrote the manuscript with contributions from all authors.

Supplemental data

The following materials are available in the online version of this article.

Supplemental Figure S1. Cu and Fe maps and Cu accumulation in the phloem exudates of wild type and the *opt3-3* mutant.

Supplemental Figure S2. The *opt3-3* mutant accumulates a high concentration of metals in vegetative tissues.

Supplemental Figure S3. The *opt3-2* mutant accumulates less Cu in roots and young leaves than wild type.

Supplemental Figure S4. OPT3 mediates Cu and Fe accumulation in developing seeds.

Supplemental Figure S5. Cellular integrity of mock and *OPT3*-expressing oocytes in control or Cu-containing solutions.

Supplemental Figure S6. *opt3* mutant seedlings are sensitive to Cu deficiency.

Supplemental Figure S7. Transferring the *opt3-3* mutant to high Cu rescues mutant growth defects.

Supplemental Figure S8. The *opt3-3* mutant accumulates IRT1 in roots under Fe-sufficient growth conditions.

Supplemental Figure S9. Phloem-feeding with carboxyfluorescein diacetate succinimidyl ester (CFDA) in leaves of wild-type Arabidopsis.

Supplemental Figure S10. Fe availability in the medium influences root and shoot growth and Fe uptake into the root but not the shoot.

Supplemental Table S1. List of primers used for RT-PCR.

Supplemental Data Set S1. Summary of RNA-seq data.

Supplemental Data Set S2. Differentially expressed genes in the roots of wild type compared to *opt3-3*.

Supplemental Data Set S3. Differentially expressed genes in the mature leaves of wild type compared to *opt3-3*.

Supplemental Data Set S4. Differentially expressed genes in the young leaves of wild type compared to *opt3-3*.

Supplemental Data Set S5. Differentially expressed genes in the roots of wild type subjected to Cu deficiency for 30 d relative to control conditions.

Supplemental Data Set S6. Summary of statistical analyses.

Funding

This study was funded by National Science Foundation Division of Integrative Organismal Systems Award #1656321 to O.K.V. and IOS #1754966 to E.W., O.K.V. and M.P.

Conflict of interest statement. None declared.

Data availability

The data that support the findings of this study are openly available in https://doi.org/10.1093/plcell/koad053.

References

Agyeman-Budu DN, Choudhury S, Coulthard I, Gordon R, Hallin E, Woll AR (2016) Germanium Collimating micro-Channel Arrays For High Resolution, High Energy Confocal X-ray Fluorescence Microscopy. Icxom23: International Conference on X-Ray Optics and Microanalysis 1764

Alexander SPH, Kelly E, Mathie A, Peters JA, Veale EL, Armstrong JF, Faccenda E, Harding SD, Pawson AJ, Sharman JL, et al. The concise guide to pharmacology 2019/20: transporters. Br J Pharmacol. 2019:**176**(S1): S397–S493 https://doi.org/10.1111/bph.14753

Araki R, Mermod M, Yamasaki H, Kamiya T, Fujiwara T, Shikanai T. SPL7 locally regulates copper-homeostasis-related genes in Arabidopsis. J Plant Physiol. 2018:**224–225**:137–143 https://doi.org/10.1016/j.jplph.2018.03.014

Arteca RN, Arteca JM. A novel method for growing Arabidopsis thaliana plants hydroponically. Physiol Plant. 2000:**108**:188–193.

Bashir K, Ishimaru Y, Itai RN, Senoura T, Takahashi M, An G, Oikawa T, Ueda M, Sato A, Uozumi N, et al. Iron deficiency regulated OsOPT7 is essential for iron homeostasis in rice. Plant Mol Biol. 2015:**88**(1-2): 165–176. https://doi.org/10.1007/s11103-015-0315-0

Baxter IR, Vitek O, Lahner B, Muthukumar B, Borghi M, Morrissey J, Guerinot ML, Salt DE. The leaf ionome as a multivariable system to detect a plant's Physiological status. Proc Natal Acad Sci U S A. 2008:**105**(33):12081–12086. https://doi.org/10.1073/pnas.0804175105

Benjamini Y, Hochberg Y. Controlling the false discovery rate: a practical and powerful approach to multiple testing. J R Stat Soc Series B Stat Methodol. 1995:**57**(1): 289–300 https://doi.org/10.1111/j.2517-6161.1995.tb02031.x

Bernal M, Casero D, Singh V, Wilson GT, Grande A, Yang H, Dodani SC, Pellegrini M, Huijser P, Connolly EL, et al. Transcriptome sequencing identifies SPL7-regulated copper acquisition genes FRO4 FRO5 and the copper dependence of iron homeostasis in Arabidopsis. Plant Cell. 2012:**24**(2):738–761. https://doi.org/10.1105/tpc.111.090431

Bogs J, Bourbouloux A, Cagnac O, Wachter A, Rausch T, Delrot S. Functional characterization and expression analysis of a glutathione transporter, BjGT1, from Brassica juncea: evidence for regulation by heavy metal exposure. Plant Cell Environ. 2003:**26**(10):1703–1711. https://doi.org/10.1046/j.1365-3040.2003.01088.x

Bolger AM, Lohse M, Usadel B. Trimmomatic: a flexible trimmer for Illumina sequence data. Bioinformatics 2014:**30**(15): 7. doi:10.1093/bioinformatics/btu170

Boyes DC, Zayed AM, Ascenzi R, McCaskill AJ, Hoffman NE, Davis KR, and Görlach J. Growth stage–based phenotypic analysis of Arabidopsis. A Model for High Throughput Functional Genomics in Plants 2001:**13**:1499–1510.

Bradford MM. A rapid and sensitive method for the quantitation of microgram quantities of protein utilizing the principle of protein-dye binding. Anal Biochem. 1976:**72**(1-2):248–254. https://doi.org/10.1016/0003-2697(76)90527-3

Broadley M, Brown P, Cakmak I, Rengel Z, Zhao F. Chapter 7-function of nutrients: micronutrients A2 - marschner, petra. Marschner's Mineral Nutrition of Higher Plants. 3rd ed. San Diego: Academic Press; 2012. p. 191–248

Burkhead JL, Gogolin Reynolds KA, Abdel-Ghany SE, Cohu CM, Pilon M. Copper homeostasis. New Phytologist. 2009:**182**(4): 799–816. https://doi.org/10.1111/j.1469-8137.2009.02846.x

Cagnac O, Bourbouloux A, Chakrabarty D, Zhang MY, Delrot S. AtOPT6 transports glutathione derivatives and is induced by primisulfuron. Plant Physiol. 2004:**135**(3):1378–1387. https://doi.org/10.1104/pp.104.039859

Cai Y, Li Y, Liang G. FIT And bHLH Ib transcription factors modulate iron and copper crosstalk in Arabidopsis. Plant Cell Environ. 2021:**44**(5):1679–1691. https://doi.org/10.1111/pce.14000

Chang CJ. Searching for harmony in transition-metal signaling. Nat Chem Biol. 2015:**11**(10):744–747. https://doi.org/10.1038/nchembio.1913

Chao Z-F, Wang Y-L, Chen Y-Y, Zhang C-Y, Wang P-Y, Song T, Liu C-B, Lv Q-Y, Han M-L, Wang S-S, et al. NPF Transporters in synaptic-like vesicles control delivery of iron and copper to seeds. Sci Adv. 2021:**7**(36):eabh2450. https://doi.org/10.1126/sciadv.abh2450

Chen C, Galon Y, Rahmati Ishka M, Malihi S, Shimanovsky V, Twito S, Rath A, Vatamaniuk OK, Miller G. Ascorbate peroxidase6 delays the onset of age-dependent leaf senescence. Plant Physiol. 2020:(2). https://doi.org/10.1093/plphys/kiaa031

Colangelo EP, Guerinot ML. The essential basic helix-loop-helix protein FIT1 Is required for the iron deficiency response. Plant Cell. 2004:**16**(12):3400–3412. https://doi.org/10.1105/tpc.104.024315

Cui Y, Chen CL, Cui M, Zhou WJ, Wu HL, Ling HQ. Four IVa bHLH transcription factors are novel interactors of FIT and mediate JA inhibition of iron uptake in Arabidopsis. Mol Plant. 2018:**11**(9): 1166–1183. https://doi.org/10.1016/j.molp.2018.06.005

Dancis A, Haile D, Yuan DS, Klausner RD. The Saccharomyces cerevisiae copper transport protein (Ctr1p). Biochemical characterization, regulation by copper, and physiologic role in copper uptake. J Biol Chem. 1994:**269**(41):25660–25667. https://doi.org/10.1016/S0021-9258(18)47300-0

Emmerstorfer A, Wriessnegger T, Hirz M, Pichler H. Overexpression of membrane proteins from higher eukaryotes in yeasts. Appl Microbiol Biotechnol. 2014:**98**(18):7671–7698. https://doi.org/10.1007/s00253-014-5948-4

Epstein E, Bloom A (2005) Mineral Nutrition of Plants: Principles and Perspectives, 2nd ed. Sunderland, Mass: Sinaur. p. 292–305

Gao F, Robe K, Bettembourg M, Navarro N, Rofidal V, Santoni V, Gaymard F, Vignols F, Roschzttardtz H, Izquierdo E, et al. The transcription factor bHLH121 interacts with bHLH105 (ILR3) and its closest homologs to regulate iron homeostasis in Arabidopsis. Plant Cell. 2020:**32**(2):508–524. https://doi.org/10.1105/tpc.19.00541

Garcia MJ, Romera FJ, Stacey MG, Stacey G, Villar E, Alcantara E, Perez-Vicente R. Shoot to root communication is necessary to control the expression of iron-acquisition genes in strategy I plants. Planta. 2013:**237**(1):65–75. https://doi.org/10.1007/s00425-012-1757-0

Gayomba SR, Jung HI, Yan J, Danku J, Rutzke MA, Bernal M, Kramer U, Kochian LV, Salt DE, Vatamaniuk OK. The CTR/COPT-dependent copper uptake and SPL7-dependent copper deficiency responses are required for basal cadmium tolerance in A. thaliana. Metallomics. 2013:**5**(9):1262–1275. https://doi.org/10.1039/c3mt00111c

Gayomba SR, Zhai Z, Jung HI, Vatamaniuk OK. Local and systemic signaling of iron status and Its interactions with homeostasis of other essential elements. Front Plant Sci. 2015:**6**:716. https://doi.org/10.3389/fpls.2015.00716

Green LS, Rogers EE. FRD3 Controls iron localization in Arabidopsis. Plant Physiol. 2004:**136**(1):2523–2531. https://doi.org/10.1104/pp.104.045633

Grignon N, Touraine B, Durand M. 6(5)Carboxyfluorescein As a tracer of phloem sap translocation. Am J Bot. 1989:**76**(6):871–877. https://doi.org/10.1002/j.1537-2197.1989.tb15064.x

Grillet L, Lan P, Li W, Mokkapati G, Schmidt W. IRON MAN is a ubiquitous family of peptides that control iron transport in plants. Nat Plants. 2018:**4**(11):953–963. https://doi.org/10.1038/s41477-018-0266-y

Grusak MA, Pezeshgi S. Shoot-to-root signal transmission regulates root Fe(III) reductase activity in the dgl mutant of pea. Plant Physiol. 1996:**110**(1):329–334. https://doi.org/10.1104/pp.110.1.329

Ha JH, Doguer C, Wang X, Flores SR, Collins JF. High-iron consumption impairs growth and causes copper-deficiency anemia in weanling sprague-dawley rats. PLoS One. 2016:**11**(8):e0161033. https://doi.org/10.1371/journal.pone.0161033

Hirayama T, Lei GJ, Yamaji N, Nakagawa N, Ma JF. The putative peptide gene FEP1 regulates iron deficiency response in Arabidopsis. Plant Cell Physiol. 2018:**59**(9):1739–1752. https://doi.org/10.1093/pcp/pcy145

Jain A, Wilson G, Connolly E. The diverse roles of FRO family metalloreductases in iron and copper homeostasis. Front Plant Sci. 2014:**5**: 100. https://doi.org/10.3389/fpls.2014.00100

Jeong J, Merkovich A, Clyne M, Connolly EL. Directing iron transport in dicots: regulation of iron acquisition and translocation. Curr Opin Plant Biol. 2017:**39**:106–113. https://doi.org/10.1016/j.pbi.2017.06.014

Jiang A, Guo Z, Pan J, Yang Y, Zhuang Y, Zuo D, Hao C, Gao Z, Xin P, Chu J, et al. The PIF1-miR408-PLANTACYANIN repression cascade regulates light-dependent seed germination. Plant Cell. 2021:**33**(5): 1506–1529. https://doi.org/10.1093/plcell/koab060

Joung J-G, Corbett AM, Fellman SM, Tieman DM, Klee HJ, Giovannoni JJ, Fei Z. Plant MetGenMAP: an integrative analysis system for plant systems biology. Plant Physiol. 2009:**151**(4):1758–1768. https://doi.org/10.1104/pp.109.145169

Jung HI, Gayomba SR, Rutzke MA, Craft E, Kochian LV, Vatamaniuk OK. COPT6 is a plasma membrane transporter that functions in copper homeostasis in *Arabidopsis* and is a novel target of SQUAMOSA promoter-binding protein-like 7. J Biol Chem. 2012:**287**(40):33252–33267. https://doi.org/10.1074/jbc.M112.397810

Jung H-I, Zhai Z, Vatamaniuk O. Direct transfer of synthetic double-stranded RNA into protoplasts of Arabidopsis thaliana. In: **Kodama H, Komamine A**, editors. RNAI and Plant Gene Function Analysis: Methods and Protocols. Totowa, NJ: Humana Press: 2011. p. 109–127

Kastoori Ramamurthy R, Xiang Q, Hsieh EJ, Liu K, Zhang C, Waters BM. New aspects of iron-copper crosstalk uncovered by transcriptomic characterization of col-0 and the copper uptake mutant spl7 in Arabidopsis thaliana. Metallomics. 2018:**10**(12):1824–1840. https://doi.org/10.1039/C8MT00287H

Khan MA, Castro-Guerrero NA, McInturf SA, Nguyen NT, Dame AN, Wang J, Bindbeutel RK, Joshi T, Jurisson SS, Nusinow DA, et al. Changes in iron availability in Arabidopsis are rapidly sensed in the leaf vasculature and impaired sensing leads to opposite transcriptional programs in leaves and roots. Plant Cell Environ. 2018:**41**(10):2263–2276. https://doi.org/10.1111/pce.13192

Kim SA, LaCroix IS, Gerber SA, Guerinot ML. The iron deficiency response in *Arabidopsis thaliana* requires the phosphorylated transcription factor URI. Proc Natal Acad Sci U S A. 2019:**116**(50): 24933–24942. https://doi.org/10.1073/pnas.1916892116

Kim SA, Punshon T, Lanzirotti A, Li L, Alonso JM, Ecker JR, Kaplan J, Guerinot ML. Localization of iron in *Arabidopsis* seed requires the vacuolar membrane transporter VIT1. Science. 2006:**314**(5803): 1295–1298. https://doi.org/10.1126/science.1132563

Kim S, Selote DS, Vatamaniuk OK. The N-terminal extension domain of the C. elegans half-molecule ABC transporter, HMT-1, is required for protein-protein interactions and function. PLoS One. 2010:**5**(9): e12938. https://doi.org/10.1371/journal.pone.0012938

Klatte M, Schuler M, Wirtz M, Fink-Straube C, Hell R, Bauer P. The analysis of Arabidopsis nicotianamine synthase mutants reveals functions for nicotianamine in seed iron loading and iron deficiency responses. Plant Physiol. 2009:**150**(1):257–271. https://doi.org/10.1104/pp.109.136374

Klevay LM. Iron overload can induce mild copper deficiency. J Trace Elem Med Biol. 2001:**14**(4):237–240. https://doi.org/10.1016/S0946-672X(01)80009-2

Knox K. Measuring phloem transport velocity in Arabidopsis seedlings using the fluorescent coumarin glucoside, esculin. In: **Liesche J**, editor. Phloem: Methods and Protocols. New York, NY: Springer; 2019. p. 195–201

Kobayashi T. Understanding the complexity of iron sensing and signaling cascades in plants. Plant Cell Physiol. 2019:**60**(7): 1440–1446. https://doi.org/10.1093/pcp/pcz038

Kumar RK, Chu H-H, Abundis C, Vasques K, Rodriguez DC, Chia J-C, Huang R, Vatamaniuk OK, Walker EL. Iron-nicotianamine transporters are required for proper long distance iron signaling. Plant Physiol. 2017:**175**(3):1254–1268. https://doi.org/10.1104/pp.17.00821

Kurt F. An insight into oligopeptide transporter 3 (OPT3) family proteins. Protein Peptide Lett. 2021:**28**(1): 43–54. https://doi.org/10.2174/0929866527666200625202028

Langmead B, Trapnell C, Pop M, Salzberg SL. Ultrafast and memory-efficient alignment of short DNA sequences to the human genome. Genome Biol. 2009:**10**(3): R25. https://doi.org/10.1186/gb-2009-10-3-r25

Li WF, Lan P. The understanding of the plant iron deficiency responses in strategy I plants and the role of ethylene in This process by omic approaches. Front Plant Sci. 2017:**8**: 40. https://doi.org/10.3389/fpls.2017.00040

Long TA, Tsukagoshi H, Busch W, Lahner B, Salt DE, Benfey PN. The bHLH transcription factor POPEYE regulates response to iron deficiency in Arabidopsis roots. Plant Cell. 2010:**22**(7):2219–2236. https://doi.org/10.1105/tpc.110.074096

Love MI, Huber W, Anders S. Moderated estimation of fold change and dispersion for RNA-seq data with DESeq2. Genome Biol. 2014:**15**(12):550. https://doi.org/10.1186/s13059-014-0550-8

Lubkowitz M. The oligopeptide transporters: a small gene family with a diverse group of substrates and functions? Mol Plant. 2011:**4**(3): 407–415. https://doi.org/10.1093/mp/ssr004

Mai HJ, Lindermayr C, von Toerne C, Fink-Straube C, Durner J, Bauer P. Iron and FER-LIKE IRON DEFICIENCY-INDUCED TRANSCRIPTION FACTOR-dependent regulation of proteins and genes in Arabidopsis thaliana roots. Proteomics. 2015:**15**(17): 3030–3047. https://doi.org/10.1002/pmic.201400351

Malzer W, Kanngießer B. A model for the confocal volume of 3D micro X-ray fluorescence spectrometer. Spectrochim Acta Part B At Spectrosc. 2005:**60**(9-10):1334–1341. https://doi.org/10.1016/j.sab.2005.07.006

Mantouvalou I, Malzer W, Kanngiesser B. Quantification for 3D micro X-ray fluorescence. Spectrochim Acta Part B At Spectrosc. 2012:**77**: 9–18. https://doi.org/10.1016/j.sab.2012.08.002

Marsch-Martínez N, Franken J, Gonzalez-Aguilera KL, de Folter S, Angenent G, Alvarez-Buylla ER. An efficient flat-surface collar-free grafting method for Arabidopsis thaliana seedlings. Plant Methods 2013:**9**(1): 14. doi:10.1186/1746-4811-9-14

Mendoza-Cózatl DG, Xie Q, Akmakjian GZ, Jobe TO, Patel A, Stacey MG, Song L, Demoin DW, Jurisson SS, Stacey G, et al. OPT3 is a component of the iron-signaling network between leaves and roots and misregulation of OPT3 leads to an over-accumulation of cadmium in seeds. Mol Plant. 2014:**7**(9):1455–1469. https://doi.org/10.1093/mp/ssu067

Morrissey J, Baxter IR, Lee J, Li L, Lahner B, Grotz N, Kaplan J, Salt DE, Guerinot ML (2009) The ferroportin metal efflux proteins function in iron and cobalt homeostasis in Arabidopsis. Plant Cell 21(10): 3326–3338 https://doi.org/10.1105/tpc.109.069401

Mukherjee I, Campbell NH, Ash JS, Connolly EL. Expression profiling of the Arabidopsis ferric chelate reductase (FRO) gene family reveals differential regulation by iron and copper. Planta. 2006:**223**(6): 1178–1190. https://doi.org/10.1007/s00425-005-0165-0

Mustroph A, Zanetti ME, Jang CJH, Holtan HE, Repetti PP, Galbraith DW, Girke T, Bailey-Serres J. Profiling translatomes of discrete cell populations resolves altered cellular priorities during hypoxia in Arabidopsis. Proc Natal Acad Sci U S A. 2009:**106**(44):18843–18848 https://doi.org/10.1073/pnas.0906131106

Newville M. Larch: An Analysis Package for XAFS and Related Spectroscopies. J. Phys.: Conf. Ser. 430. 2013

Nguyen NT, Khan MA, Castro-Guerrero NA, Chia J-C, Vatamaniuk OK, Mari S, Jurisson SS, Mendoza-Cozatl DG. Iron availability within the leaf vasculature determines the magnitude of iron deficiency responses in source and sink tissues in Arabidopsis. Plant Cell Physiol. 2022:**63**(6): 829–841https://doi.org/10.1093/pcp/pcac046

Oparka KJ, Duckett CM, Prior DAM, Fisher DB. Real-time imaging of phloem unloading in the root tip of Arabidopsis. Plant J. 1994:**6**(5): 759–766. https://doi.org/10.1046/j.1365-313X.1994.6050759.x

Oparka KJ, Prior DAM, Wright KM. Symplastic communication between primary and developing lateral roots of Arabidopsis thaliana. J Exp Bot. 1995:**46**(2):187–197. https://doi.org/10.1093/jxb/46.2.187

Osawa H, Stacey G, Gassmann W. ScOPT1 and AtOPT4 function as proton-coupled oligopeptide transporters with broad but distinct substrate specificities. Biochem J. 2006:**393**(1):267–275. https://doi.org/10.1042/BJ20050920

Perez-Anton M, Schneider I, Kroll P, Hofhuis H, Metzger S, Pauly M, Hay A. Explosive seed dispersal depends on SPL7 to ensure sufficient copper for localized lignin deposition via laccases. Proc Natl Acad Sci U S A. 2022:**119**(24):e2202287119. https://doi.org/10.1073/pnas.2202287119

Pilon M. The copper microRNAs. New Phytol. 2017:**213**(3):1030–1035. https://doi.org/10.1111/nph.14244

Pottier M, Dumont J, Masclaux-Daubresse C, Thomine S. Autophagy is essential for optimal translocation of iron to seeds in Arabidopsis. J Exp Bot. 2019:**70**(3): 859–869 https://doi.org/10.1093/jxb/ery388

Quast C, Pruesse E, Yilmaz P, Gerken J, Schweer T, Yarza P, Peplies J, Glöckner FO. The SILVA ribosomal RNA gene database project: improved data processing and web-based tools. Nucleic Acids Res. 2013:**41**(D1): 7. https://doi.org/10.1093/nar/gks1219

Rahmati Ishka M, Chia J-C, Vatamaniuk OK. Chapter 12- advances in understanding of copper function and transport in plants. In: **Upadhyay SK**, editor. Cation Transporters in Plants. 2022. Academic Press. p. 205–226

Rahmati Ishka M, Vatamaniuk OK. Copper deficiency alters shoot architecture and reduces fertility of Both gynoecium and androecium in Arabidopsis thaliana. Plant Direct. 2020:**4**(11):e00288. https://doi.org/10.1002/pld3.288

Rai S, Singh PK, Mankotia S, Swain J, Satbhai SB. Iron homeostasis in plants and its crosstalk with copper, zinc, and manganese. Plant Stress. 2021:**1**:100008. https://doi.org/10.1016/j.stress.2021.100008

Ravet K, Pilon M. Copper and iron homeostasis in plants: the challenges of oxidative stress. Antioxidants Redox Signal. 2013:**19**(9): 23. https://doi.org/10.1089/ars.2012.5084

Rees EM, Lee J, Thiele DJ. Mobilization of intracellular copper stores by the Ctr2 vacuolar copper transporter. J Biol Chem. 2004:**279**(52): 54221–54229. https://doi.org/10.1074/jbc.M411669200

Rellán-Álvarez R, Giner-Martínez-Sierra J, Orduna J, Orera I, Rodríguez-Castrillón JÁ, García-Alonso JI, Abadía J, Álvarez-Fernández A. Identification of a tri-iron(III), tri-citrate Complex in the Xylem sap of iron-deficient tomato resupplied with iron: new insights into plant iron long-distance transport. Plant Cell Physiol. 2009:**51**(1):91–102. https://doi.org/10.1093/pcp/pcp170

Rodríguez FI, Esch JJ, Hall AE, Binder BM, Schaller GE, Bleecker AB. A copper cofactor for the ethylene receptor ETR1 from *Arabidopsis*. Science. 1999:**283**(5404):996–998. https://doi.org/10.1126/science.283.5404.996

Rogers EE, Guerinot ML. FRD3, A member of the multidrug and toxin efflux family, controls iron deficiency responses in Arabidopsis. Plant Cell. 2002:**14**(8):1787–1799. https://doi.org/10.1105/tpc.001495

Ross-Elliott TJ, Jensen KH, Haaning KS, Wager BM, Knoblauch J, Howell AH, Mullendore DL, Monteith AG, Paultre D, Yan D, et al. Phloem unloading in Arabidopsis roots is convective and regulated by the phloem-pole pericycle. eLife. 2017:**6**:e24125. https://doi.org/10.7554/eLife.24125

Schott-Verdugo S, Müller L, Classen E, Gohlke H, Groth G. Structural model of the ETR1 ethylene receptor transmembrane sensor domain. Sci Rep. 2019:**9**(1):8869. https://doi.org/10.1038/s41598-019-45189-w

Schulten A, Pietzenuk B, Quintana J, Scholle M, Feil R, Krause M, Romera-Branchat M, Wahl V, Severing E, Coupland G, et al. Energy status-promoted growth and development of Arabidopsis require copper deficiency response transcriptional regulator SPL7. Plant Cell. 2022:**34**(10):3873–3898. https://doi.org/10.1093/plcell/koac215

Schwarz B, Bauer P. FIT, a regulatory hub for iron deficiency and stress signaling in roots, and FIT-dependent and -independent gene signatures. J Exp Bot. 2020:**71**(5):1694–1705. https://doi.org/10.1093/jxb/eraa012

Selote D, Samira R, Matthiadis A, Gillikin JW, Long TA. Iron-binding E3 ligase mediates iron response in plants by targeting basic Helix-loop-Helix transcription factors. Plant Physiol. 2014:**167**(1): 273–286. https://doi.org/10.1104/pp.114.250837

Shaff JE, Schultz BA, Craft EJ, Clark RT, Kochian LV. GEOCHEM-EZ: a chemical speciation program with greater power and flexibility. Plant Soil. 2010:**330**(1-2):207–214. https://doi.org/10.1007/s11104-009-0193-9

Sheng H, Jiang Y, Ishka MR, Chia JC, Dokuchayeva T, Kavulych Y, Zavodna TO, Mendoza PN, Huang R, Smieshka LM, et al. YSL3-mediated Copper distribution is required for fertility, seed size and protein accumulation in Brachypodium. Plant Physiol. 2021:**186**(1):655–676. https://doi.org/10.1093/plphys/kiab054

Sivitz A, Grinvalds C, Barberon M, Curie C, Vert G. Proteasome-mediated turnover of the transcriptional activator FIT is required for plant iron-deficiency responses. Plant J. 2011:**66**(6):1044–1052. https://doi.org/10.1111/j.1365-313X.2011.04565.x

Solé VA, Papillon E, Cotte M, Walter P, Susini J. A multiplatform code for the analysis of energy-dispersive X-ray fluorescence spectra. Spectrochim Acta Part B At Spectrosc. 2007:**62**(1):63–68. https://doi.org/10.1016/j.sab.2006.12.002

Spielmann J, Vert G. The many facets of protein ubiquitination and degradation in plant root iron-deficiency responses. J Exp Bot. 2020:**72**(6):2071–2082. https://doi.org/10.1093/jxb/eraa441

Stacey MG, Koh S, Becker J, Stacey G. AtOPT3, a member of the oligopeptide transporter family, is essential for embryo development in Arabidopsis. Plant Cell. 2002:**14**(11):2799–2811. https://doi.org/10.1105/tpc.005629

Stacey MG, Patel A, McClain WE, Mathieu M, Remley M, Rogers EE, Gassmann W, Blevins DG, Stacey G. The Arabidopsis AtOPT3 protein functions in metal homeostasis and movement of iron to developing seeds. Plant Physiol. 2008:**146**(2):589–601. https://doi.org/10.1104/pp.107.108183

Trapnell C, Pachter L, Salzberg SL. Tophat: discovering splice junctions with RNA-seq. Bioinformatics. 2009:**25**(9):7. https://doi.org/10.1093/bioinformatics/btp120

Tsang T, Posimo JM, Gudiel AA, Cicchini M, Feldser DM, Brady DC. Copper is an essential regulator of the autophagic kinases ULK1/2 to drive lung adenocarcinoma. Nat Cell Biol. 2020:**22**(4):412–424. https://doi.org/10.1038/s41556-020-0481-4

Turski ML, Brady DC, Kim HJ, Kim BE, Nose Y, Counter CM, Winge DR, Thiele DJ. A novel role for copper in Ras/mitogen-activated protein kinase signaling. Mol Cell Biol. 2012:**32**(7):1284–1295. https://doi.org/10.1128/MCB.05722-11

Turski ML, Thiele DJ. New roles for copper metabolism in cell proliferation, signaling, and disease. J Biol Chem. 2009:**284**(2):717–721. https://doi.org/10.1074/jbc.R800055200

Vatamaniuk OK. Plant movement and LAC of it: how copper facilitates explosive seed dispersal. Proc Natl Acad Sci U S A. 2022:**119**(28):e2208331119. https://doi.org/10.1073/pnas.2208331119

Vert GA, Briat J-F, Curie C. Dual regulation of the Arabidopsis high-affinity root iron uptake system by local and long-distance signals. Plant Physiol. 2003:**132**(2):796–804. https://doi.org/10.1104/pp.102.016089

Waters BM, Armbrust LC. Optimal copper supply Is required for normal plant iron deficiency responses. Plant Signal Behav. 2013:**8**(12):e26611. https://doi.org/10.4161/psb.26611

Waters BM, McInturf SA, Amundsen K. Transcriptomic and physiological characterization of the FeFe mutant of melon (Cucumis melo) reveals new aspects of iron-copper crosstalk. New Phytol. 2014:**203**(4):1128–1145. https://doi.org/10.1111/nph.12911

Waters BM, McInturf SA, Stein RJ. Rosette iron deficiency transcript and microRNA profiling reveals links between copper and iron homeostasis in Arabidopsis thaliana. J Exp Bot. 2012:**63**(16):5903–5918. https://doi.org/10.1093/jxb/ers239

Wongkaew A, Asayama K, Kitaiwa T, Nakamura SI, Kojima K, Stacey G, Sekimoto H, Yokoyama T, Ohkama-Ohtsu N. AtOPT6 protein functions in long-distance transport of glutathione in Arabidopsis thaliana. Plant Cell Physiol. 2018:**59**(7):1443–1451. https://doi.org/10.1093/pcp/pcy074

Wu Y, Zhang D, Chu Jee Y, Boyle P, Wang Y, Brindle Ian D, De Luca V, Després C. The Arabidopsis NPR1 protein is a receptor for the plant defense hormone salicylic acid. Cell Rep. 2012:**1**(6):639–647. https://doi.org/10.1016/j.celrep.2012.05.008

Yamasaki H, Hayashi M, Fukazawa M, Kobayashi Y, Shikanai T. SQUAMOSA Promoter binding protein-like7 is a central regulator for copper homeostasis in *Arabidopsis*. Plant Cell. 2009:**21**(1):347–361. https://doi.org/10.1105/tpc.108.060137

Yan J, Chia J-C, Sheng H, Jung H-I, Zavodna T-O, Zhang L, Huang R, Jiao C, Craft EJ, Fei Z, et al. Arabidopsis pollen fertility requires the transcription factors CITF1 and SPL7 that regulate copper delivery to anthers and jasmonic acid synthesis. Plant Cell. 2017:**29**(12):3012–3029. https://doi.org/10.1105/tpc.17.00363

Zhai Z, Gayomba SR, Jung H-I, Vimalakumari NK, Piñeros M, Craft E, Rutzke MA, Danku J, Lahner B, Punshon T, et al. OPT3 is a phloem-specific iron transporter that is essential for systemic iron signaling and redistribution of iron and cadmium in Arabidopsis. Plant cell. 2014:**26**(5):2249–2264. https://doi.org/10.1105/tpc.114.123737

Zhang Z, Xie Q, Jobe TO, Kau AR, Wang C, Li Y, Qiu B, Wang Q, Mendoza-Cózatl DG, Schroeder JI. Identification of AtOPT4 as a plant glutathione transporter. Mol Plant. 2016:**9**(3):481–484. https://doi.org/10.1016/j.molp.2015.07.013

Zhong S, Joung J-G, Zheng Y, Chen Y-R, Liu B, Shao Y, Xiang JZ, Fei Z, Giovannoni JJ. High-throughput illumina strand-specific RNA sequencing library preparation. Cold Spring Harb Protoc. 2011:**2011**(8):940–949. https://doi.org/10.1101/pdb.prot5652